Nano Today 29 (2019) 100797

Contents lists available at ScienceDirect

Nano Today

journal homepage: www.elsevier.com/locate/nanotoday

Review

Recent advances in upconversion nanocrystals: Expanding the kaleidoscopic toolbox for emerging applications

Kezhi Zheng[a,*], Kang Yong Loh[b], Yu Wang[c], Qiushui Chen[a], Jingyue Fan[a], Taeyoung Jung[d,e], Sang Hwan Nam[e,f], Yung Dong Suh[e,g,**], Xiaogang Liu[a,c,*]

[a] Department of Chemistry, National University of Singapore, 3 Science Drive 3, Singapore 117543, Singapore
[b] Institute of Materials Research and Engineering, Agency for Science, Technology and Research (A*STAR), Innovis, 138634, Singapore
[c] SZU-NUS Collaborative Center and International Collaborative Laboratory of 2D Materials for Optoelectronic Science & Technology of Ministry of Education, Institute of Microscale Optoelectronics, Shenzhen University, Shenzhen 518060, China
[d] Department of Chemistry, Gwangju Institute of Science and Technology (GIST), Gwangju 61005, South Korea
[e] Research Center for Convergence NanoRaman Technology, Korea Research Institute of Chemical Technology, Daejeon 34114, South Korea
[f] Center for Convergent Research of Emerging Virus Infection, Korea Research Institute of Chemical Technology, Daejeon 34114, South Korea
[g] School of Chemical Engineering, Sung Kyun Kwan University (SKKU), Suwon 16419, South Korea

ARTICLE INFO

Article history:
Received 3 May 2019
Received in revised form 5 August 2019
Accepted 30 September 2019
Available online 16 November 2019

Keywords:
Lanthanide
Upconversion nanoparticles
Synthesis
Multicolour
Luminescence enhancement
Application

ABSTRACT

Lanthanide-doped upconversion nanoparticles enable anti-Stokes emission *via* nonlinear processes, where low-energy excitation photons in the near-infrared window can be upconverted into high-energy emission ones in the visible or ultraviolet regions. The past decade has seen great success in the high-quality synthesis of upconversion nanoparticles with controlled structure, crystalline phase, size, and shape. The unique capacity of upconversion nanocrystals to undertake near-infrared excitation, amalgamated with their excellent luminescent characteristics, such as massive anti-Stokes spectral shift, sharp emission band, multicolor emission, and long luminescence lifetime, makes these nanomaterials prime candidates for a plethora of applications. Herein, we review the field of upconversion nanoparticles from the perspectives of fundamental luminescence mechanisms, new synthetic routes, and current practical approaches to tuning emission color and enhancing upconversion efficiency. In particular, we highlight the recent advances in utilizing upconversion nanocrystals for bioimaging, therapy, biosensing, neuroscience, super-resolution imaging, photoswitching, and lasing applications. We also discuss the key challenges and issues that are critical for the further implementation of upconversion nanoparticles in diverse settings.

Contents

* Corresponding authors.
** Corresponding author at: Research Center for Convergence NanoRaman Technology, Korea Research Institute of Chemical Technology, Daejeon 34114, South Korea.
E-mail addresses: chmzhke@nus.edu.sg (K. Zheng), ydsuh@krict.re.kr (Y.D. Suh), chmlx@nus.edu.sg (X. Liu).

https://doi.org/10.1016/j.nantod.2019.100797
1748-0132/

Introduction

Lanthanide ion (Ln^{3+})-mediated photon upconversion refers to a unique nonlinear process in which two or more near-infrared (NIR) pump photons are absorbed through real intermediate energy levels of Ln^{3+}, leading to the emission of light at a wavelength shorter than incident radiation. In the 1960s, this phenomenon was first discovered and formulated in bulk materials by Auzel, Ovsyankin and Feofilov independently [1,2]. Since then, tremendous research efforts have been paid to Ln^{3+}-doped upconversion luminescence owing to its remarkable optical properties such as large anti-Stokes shift, long luminescence lifetime, and tunable emission profile [3–6]. In comparison with well-established two-photon absorption (TPA) and second-harmonic generation (SHG) where high-power density (>10^6 W/cm^2) photon flux produced by expensive ultra-short pulsed lasers are needed to perform upconversion, Ln^{3+}-doped photon upconversion can be activated upon irradiation with a low-cost continuous-wave (c.w.) NIR diode laser or an incoherent light source at low pumping density (~10^{-1} W/cm^2) [7,8]. Moreover, the lanthanides' partially filled 4*f* shells are effectively shielded by outer complete 5*s* and 5*p* shells, leading to sharp emission peaks due to intra-4*f* electron transitions. All these unique features make Ln^{3+}-doped upconversion materials ideal candidates for diverse applications, ranging from biomedicine and super-resolution imaging to volumetric displays and photovoltaics [9–12].

Despite its promise, the investigation of Ln^{3+}-doped upconversion luminescence has been mainly focused on bulk materials or glass ceramics for the first few decades after its discovery [13–15]. It was not until the late 1990s, when nanoscience and nanotechnology became prevalent in the field of materials science, that high-quality upconversion nanoparticles (UCNPs) with controllable composition, crystalline phase, size, and shape were routinely synthesized. The advent of these nanomaterials provides a new platform that significantly expands the repertoire of the luminescence toolbox available for advanced nanophotonic and biological research [16–20]. With the growing awareness of drawbacks associated with traditional downshifting fluorescent dyes and semiconductor quantum dots such as photobleaching, cytotoxicity and the need for high-energy ultraviolet or blue stimulation, Ln^{3+}-doped UCNPs featuring small size, low toxicity and excellent biocompatibility alongside high photostability are particularly attractive as luminescence probes for bioimaging applications [21–25].

To date, the biggest challenge that limits the further application of Ln^{3+}-doped UCNPs is their low quantum efficiency. Owing to the low extinction coefficients of lanthanides and small size-induced surface quenching effects, the quantum yield of Ln^{3+}-doped UCNPs is typically less than 1% [26,27]. Although several approaches and proposals have been shown effective in enhancing the luminescence brightness of UCNPs, the fundamental mechanisms underlying the upconversion pathways are not entirely clear.

In this review, we focus on the controllable preparation, luminescence performance optimization and emerging applications of Ln^{3+}-doped UCNPs. The review is divided into four main sections. Firstly, we briefly introduce the fundamentals governing Ln^{3+}-doped upconversion phenomena, including different types of upconversion mechanisms and electronic transitions between energy levels. In the following section, we attempt to highlight general strategies for the controllable synthesis of UCNPs. Next, we give an overview of tuning mechanisms of upconversion luminescence and summarize current approaches to enhancing photon upconversion. Finally, we highlight the recent success of using UCNPs in developing emerging applications and provide a perspective on design strategies for the optimization of energy harvesting to maximize luminescence amplification.

Upconversion luminescence of lanthanide-doped nanoparticles

Upconversion luminescence generally comes from electronic transitions within lanthanide's $4f^N$ configuration. Although these electronic transitions are in principle forbidden by quantum mechanical selection rules, they can occur by intermixing higher electronic configurations with *f* states. More interestingly, the lanthanide's $4f^N$ electronic configuration could split into an abundance of energy sublevels as a result of strong Coulombic interactions and spin-orbit coupling as well as weak perturbations in the crystal field, leading to a plentiful of emission bands from the optical transitions among these levels (Fig. 1a) [8].

Mechanism

In general, lanthanide-based upconversion processes can be categorized into six classes: excited-state absorption (ESA), energy transfer upconversion (ETU), cooperative upconversion (CUC), cross-relaxation (CR), photon avalanche (PA), and energy migration-mediated upconversion (EMU) (Fig. 1b) [1,28].

ESA features a population mechanism where the successive absorption of pumping photons by a single ion (I) leads to electronic transitions from the ground state to high-energy excited states. Ladder-like arranged and near evenly-spaced energy levels of Ln^{3+} ions are required to achieve efficient ESA. Such energy level structures can only be observed in a small set of lanthanides such as Ho^{3+}, Er^{3+} and Tm^{3+}, which are suitable luminescence centers for ESA process to proceed [29–32].

Similar to ESA, ETU process takes advantage of sequential absorption of excitation photons to populate the intermediate levels of lanthanide dopant. However, the ETU process involves the participation of two types of neighboring ions, namely sensitizer (I) and activator (II). Because the absorption cross-section of Yb^{3+} at 980 nm matches well with the operating wavelength of the commercially available diode laser, Yb^{3+} ions are commonly used as sensitizers in the ETU process [33–35]. In addition, the efficiency of

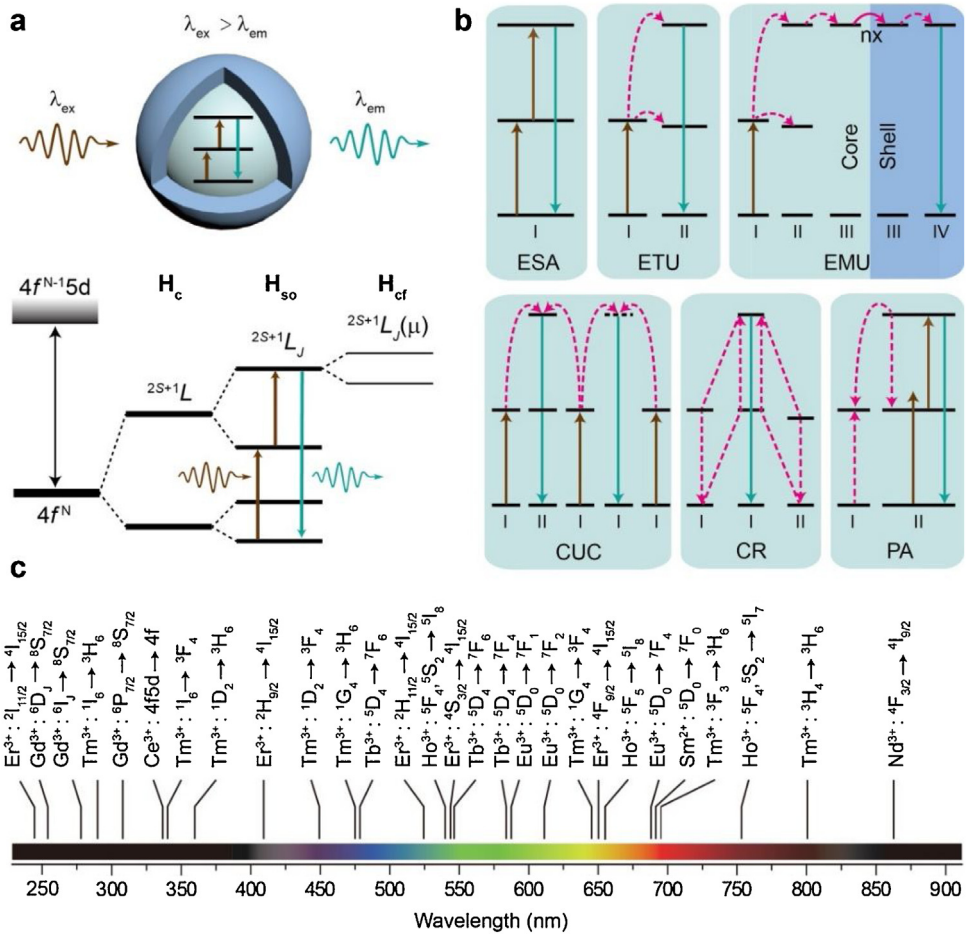

Fig. 1. (a) Schematic illustration of a core-shell-structured upconversion nanoparticle, which features a typical anti-Stokes emission with photon energy higher than the excitation light ($\lambda_{ex} > \lambda_{em}$) (top) and the simplified electronic energy level diagrams of lanthanide ions in relation to a simple upconversion process (bottom). The $4f^N$ electronic configuration of lanthanide ions splits into many energy sublevels owing to the strong effects of the Coulombic field (H_c), spin-orbit coupling (H_{so}), and weak crystal-field interaction (H_{cf}). The energy levels are represented in the form of $^{2S+1}L_J$, where S refers to total spin angular momentum, L the total orbital angular momentum, and J specifies the total angular momentum quantum number of the electron. (b) Principal upconversion mechanisms of lanthanide-doped nanocrystals. ESA, ETU, EMU, CUC, CR and PA represents excited state absorption, energy transfer upconversion, energy migration-mediated upconversion, cooperative upconversion (including cooperative luminescence and cooperative sensitization), cross-relaxation and photon avalanche, respectively. (c) Typical electronic transitions of lanthanide ions covering a broad range of wavelengths from ultraviolet to near-infrared region.

an ETU process is determined by the average distance between the sensitizer and activator, which is dependent on doping concentrations.

CUC is a three-body or four-body process in which the population of emitting levels usually arises from cooperative energy transfer of adjacent ions. CUC generally covers cooperative luminescence and cooperative sensitization. In the case of cooperative luminescence, the energy donor (I) and acceptor (I) are of the same type of lanthanide ions, *e.g.,* Yb^{3+}-Yb^{3+} ion pair. Although cooperative luminescence of three Yb^{3+} ions has been observed in the UV region, it was only limited to bulk material [36]. As for the cooperative sensitization, these two participants refer to different lanthanide dopants (I and II), *e.g.,* Yb^{3+}-Eu^{3+}, Yb^{3+}-Tb^{3+}, and Yb^{3+}-Pr^{3+} ion pairs [37,38]. Due to the involvement of virtual pair levels during electronic transitions, a lower efficiency was typically observed in CUC (10^{-6}) than that of ESA and ETU processes.

Cross-relaxation is a form of energy transfer process that occurs between the same (I and I) or different (I and II) types of activators if their optical transitions match well with each other. Although cross-relaxation had always been regarded as the main reason for deleterious concentration quenching, it can also be intentionally utilized as a beneficial modulator for tuning emission profiles in some cases. For instances, by importing Ce^{3+} into Yb^{3+}-Ho^{3+} codoped materials and utilizing the CR between Ho^{3+} and Ce^{3+}, one can tune the upconversion radiation of Ho^{3+} from green to red [11,39].

In the case of PA, excitation intensity above a certain threshold is a prerequisite. This phenomenon was first discovered in Pr^{3+}-doped infrared quantum counters [40]. The weak ground state absorption, strong excited state absorption, and efficient cross-relaxation are three essential factors for inducing photon avalanche upconversion. Owing to the feedback looping of excited state absorption along with cross-relaxation, PA exhibits the highest efficiency in photon upconversion. However, its disadvantages, such as high excitation threshold and long rise time, limit its widespread applications.

The phenomenon of EMU is governed by a novel upconversion mechanism that requires four kinds of lanthanide dopants and a core-shell layout [41,42]. In the EMU process, a sensitizer (I) first absorbs NIR excitation photons and conducts energy transfers successively from the excited sensitizer (I) to the accumulator (II). Following which, a migrator ion (III), usually Gd^{3+} ion, obtains the excitation energy from the accumulator in the neighboring site, continued with the random energy hopping throughout the core-shell interface. Finally, the activator ion (IV) captures the migrating energy to induce upconverted emission. The core-shell structure

and arrangement of migrator ions at the core-shell interface are beneficial for minimizing luminescence quenching and facilitating the energy transfer between the accumulator and activator, which is essential to generate an efficient EMU process.

Host, sensitizer, and activator

An inorganic UCNP typically comprises an inorganic host matrix and trivalent lanthanide dopant accommodated in the host lattice. The screening of an appropriate host matrix is critical for synthesizing high-quality upconversion nanoparticles with desirable optical properties such as high quantum efficiency and controllable luminescence profile. Host materials with low phonon energies, such as fluorides ($\sim$350 cm^{-1}), are optimal candidates for photon upconversion due to their abilities to minimize non-radiative energy losses during upconversion processes. In addition to phonon energy, the crystal structure of host material has a significant influence on the efficiency of upconversion luminescence as well. Generally, selecting host materials with low symmetry is more favorable to achieve efficient upconversion luminescence than that of host lattices with high symmetry. For example, upconversion efficiency of β-$NaYF_4$:Yb/Er bulk material is about 10 times higher than that of its cubic counterparts [16]. Recently, several novel upconversion host materials, such as hexagonal-phase $NaLuF_4$, tetragonal-phase $LiLuF_4$, even $CsPbCl_3$ perovskite nanocrystals, have been found to yield efficient upconversion output [43–45]. Although related photophysical mechanisms need to be further clarified, these studies will encourage researchers to seek more efficient host matrices for photon upconversion.

Lanthanide luminescent ions have small absorption cross-sections in the NIR region, resulting in relatively low upconversion efficiency in singly doped nanoparticles. To enhance upconversion quantum efficiency, a sensitizer is usually codoped with the activator in a typical upconversion nanoparticle to increase the NIR absorption. For example, Yb^{3+} ion, with a broad absorption cross-section at 980 nm, is usually used as a sensitizer ion in Yb^{3+}-Er^{3+}, Yb^{3+}-Tm^{3+}, or Yb^{3+}-Ho^{3+} codoped materials [33–35]. Nd^{3+} is another important sensitizer with its efficient absorption locates at $\sim$800 nm. Compared with Yb^{3+}-based upconversion nanoparticles where a 980 nm laser is served as pumping source, Nd^{3+}-sensitized systems can facilitate photon upconversion at a biocompatible excitation wavelength with significantly minimize the overheating problem. This characteristic makes Nd^{3+}-sensitized upconversion nanoparticles ideal candidates for biological applications [46,47]. In addition to lanthanide dopants, organic dyes have emerged in recent years as a new kind of sensitizers for upconversion owing to their broadband and intense absorption. By employing organic dyes as antennae and utilizing Förster resonance energy transfer (FRET) from dye ligands to lanthanide dopants, NIR excitation energy can be efficiently harvested to produce photon upconversion [48–54].

In upconversion nanoparticles, lanthanide ions that feature ladder-like electronic levels are usually co-doped as activators for an upconversion process to proceed. Prior to the discovery of the EMU process, the efficient activators have only been limited to Er^{3+}, Tm^{3+}, and Ho^{3+}, but recently they have expanded to Ce^{3+}, Gd^{3+}, Tb^{3+}, Dy^{3+}, Eu^{3+}, and Sm^{3+} ions in core-shell-designed upconversion nanocrystals [41]. More interestingly, transition metal ions Mn^{2+} and Cu^{2+}, metal ion Pb^{2+} and even the lanthanide divalent ion Sm^{2+} have also proven to be potent activators for upconversion luminescence, which largely broadens the range of upconversion luminous centers [55–58]. By properly selecting the type of lanthanide dopants in a nanoparticle, one can precisely modulate the emission wavelength of Ln^{3+}-doped UCNPs spanning the spectrum from UV and visible to NIR windows (Fig. 1c).

Design and synthesis of lanthanide-doped upconversion nanoparticles

To date, many chemical techniques have been developed to synthesize Ln^{3+}-doped upconversion nanocrystals with controllable structures, sizes, and shapes (Table 1). Among these methods, hydro(solvo)thermal synthesis, coprecipitation and thermal decomposition are the three most popular approaches for producing high-quality upconversion nanoparticles (Fig. 2). In this section, we will summarize systematically strategies used for controllable synthesis of Ln^{3+}-doped UCNPs.

Hydro(solvo)thermal synthesis

Hydrothermal synthesis refers to a method to grow crystalline material from an aqueous solution at high temperature and high vapor pressure. The main difference between solvothermal and hydrothermal process is that the precursor solution is usually non-aqueous for solvothermal synthesis. A specially-made autoclave is generally utilized during hydro(solvo)thermal reaction process. Hydro(solvo)thermal process features a controllable synthesis strategy in which crystalline phase, size, and morphology of synthesized nanoparticles are influenced by reactant concentration, reaction temperature, time, pH value, and solvent/surfactant types. For example, based on hydro(solvo)thermal method, Li and co-workers have developed a “liquid-solid-solution (LSS)” strategy to synthesize many different monodispersed nanocrystals, including semiconductor, metal and dielectric materials [59]. Adapted from this method, a variety of high-quality fluoride matrices, such as $NaYF_4$, $NaGdF_4$, YF_3, LaF_3, $BaGdF_5$, CaF_2, have been synthesized as well (Fig. 2a–d) [60–62]. Another significant progress by using oleic acid-mediated hydrothermal method was reported by Zhao et al. to generate uniform $NaYF_4$ nanorods, nanocubes, and flower-patterned nanodisks under different reaction conditions [63]. Recently, Liu and co-workers developed a novel Gd^{3+}-codoped strategy to control the size and crystalline phase of $NaYF_4$ nanocrystals simultaneously [17]. By doping Gd^{3+} ions into the reaction solution during the solvothermal process, a rapid cubic-to-hexagonal phase transformation is implemented, leading to the production of small-sized $NaYF_4$ nanocrystals at relatively low reaction temperatures. The similar phenomena of doping-induced phase and size changes have also been verified in other host materials [64,65]. Besides the aforementioned fluoride-based upconversion nanoparticles, lanthanide-doped oxide nanoparticles with controllable size and shape such as Er_2O_3, $YbPO_4$, $LuPO_4$, and $GdVO_4$, have also been successfully prepared using the hydro(solvo)thermal method [66,67].

Coprecipitation

Coprecipitation is an excellent synthetic method for which high purity and precise stoichiometric control are required. Compared to other techniques, coprecipitation is more convenient for synthesizing lanthanide-doped nanocrystals because it avoids the use of expensive equipment and complex procedures. By employing this method, van Veggel and co-workers have synthesized Ln^{3+}-doped LaF_3 nanocrystals for the first time [68]. This approach was subsequently refined by Chow et al. to prepare upconversion nanocrystals with small particle size and narrow size distribution. [69]. The ammonium di-*n*-octadecyldithiophosphate (ADDP) was employed as a surfactant in their studies for the controllable growth of nanoparticles without aggregation. In addition to ADDP, polyethylenimine (PEI) and polyvinylpyrrolidone (PVP) can also be used as surfactants during particle growth to endow the resulting nanoparticles with high solubility and surface functionality. Coupled with heat treatment, the coprecipitation method

Table 1
Typical synthetic strategies to lanthanide-doped upconversion nanocrystals.

Synthesis strategy	Host	Advantages & Disadvantages
Hydro(solvo)thermal synthesis	Na(Y, Gd, Yb, Lu)F_4, $LiYF_4$, $La_2(MoO_4)_3$, (La, Y)$_2O_3$, (La, Y, Gd, Lu)F_3, Ba(Y, Gd)F_5, BaY_2F_5, Ba_2GdF_7, (Ca, Sr)F_2, Sr_2ScF_7, (Y, Yb)PO_4, $Y_3Al_5O_{12}$, MnF_2, $KMnF_3$, $GdVO_4$, $PbTiO_3$, $KNbO_3$, Gd_2O_2S, *etc.*	Formation of highly crystalline phases at much lower temperature. Excellent control over particle size and shape. Specialized autoclaves required. Impossibility of observing the crystal as it grows.
Coprecipitation	Na(La, Y, Gd, Yb, Lu, Sc, Tb)F_4, (La, Y, Gd, Lu)F_3, Li(Y, Gd, Yb, Lu)F_4, (Ca, Sr)F_2, $BaYF_5$, GdOF, (La, Y, Yb, Lu)PO_4, ZrO_2, Y_2O_2S, ZnO, $Gd_4O_3F_6$, $CaMoO_4$, $Y_3Al_5O_{12}$, Y_4MoO_9, $Y_2(MoO_4)_3$, $Gd_2(WO_4)_3$, $Gd_3Ga_5O_{12}$, $BaTiO_3$, Y_2SiO_5, *etc.*	Simple and rapid preparation. Fast growth rate. Easy control of particle size and composition. Low product yield. Particle aggregation. Post-heat treatment typically need.
Thermal decomposition	LaF_3, Na(Y, Gd, Yb, Lu)F_4, Li(Y, Lu)F_4, (La, Y, Tb, Ho, Er, Tm, Yb, Lu)$_2O_3$, Ba(Y, Gd, Lu)F_5, CaF_2, $BaTiO_3$, YOF, (La, Gd)OL, *etc.*	High quality, monodisperse nanocrystals. Rigorous and harsh synthesis condition. Hydrophobic resultants. Toxic by-products.
Sol-gel	(La, Y)F_3, CaF_2, LaOF, (Y, Gd)$_2O_3$, TiO_2, ZnO, Ta_2O_5, GeO_2, Al_2O_3, $BaTiO_3$, LaPO4, (Gd, Lu)$_3Ga_5O_{12}$, YVO_4, ZrO_2, Y_2SiO_5, $Y_2Ti_2O_7$, $BaGd_2(MoO_4)_4$, $CaGd_2(WO_4)_4$, *etc.*	Simple and cost-effective accessories. Versatile. Better homogeneity. Less energy consumption. Cost of precursors. High-temperature post-heat treatment required.
Ionic liquid-based synthesis	Na(Y, Gd, Yb)F_4, (La, Y)F_3, CaF_2, $BaMgF_4$, *etc.*	Easy processing. Low solvent toxicity. Ratively expensive. Poorly biodegradable.
Microwave-assisted synthesis	(La, Gd)F_3, Na(Y, Gd)F_4, CaF_2, $BaYF_5$, $LaPO_4$, (Ca, Sr, Ba)MoO_4, Ca(La, Gd)$_2(MoO_4)_4$, $NaLa(MoO_4)_2$, $NaY(WO_4)_2$, $SrY_2(MoO_4)_4$, *etc.*	Uniform heating. Rapid synthesis. Higher product yields. Specialized microwave reactor required.

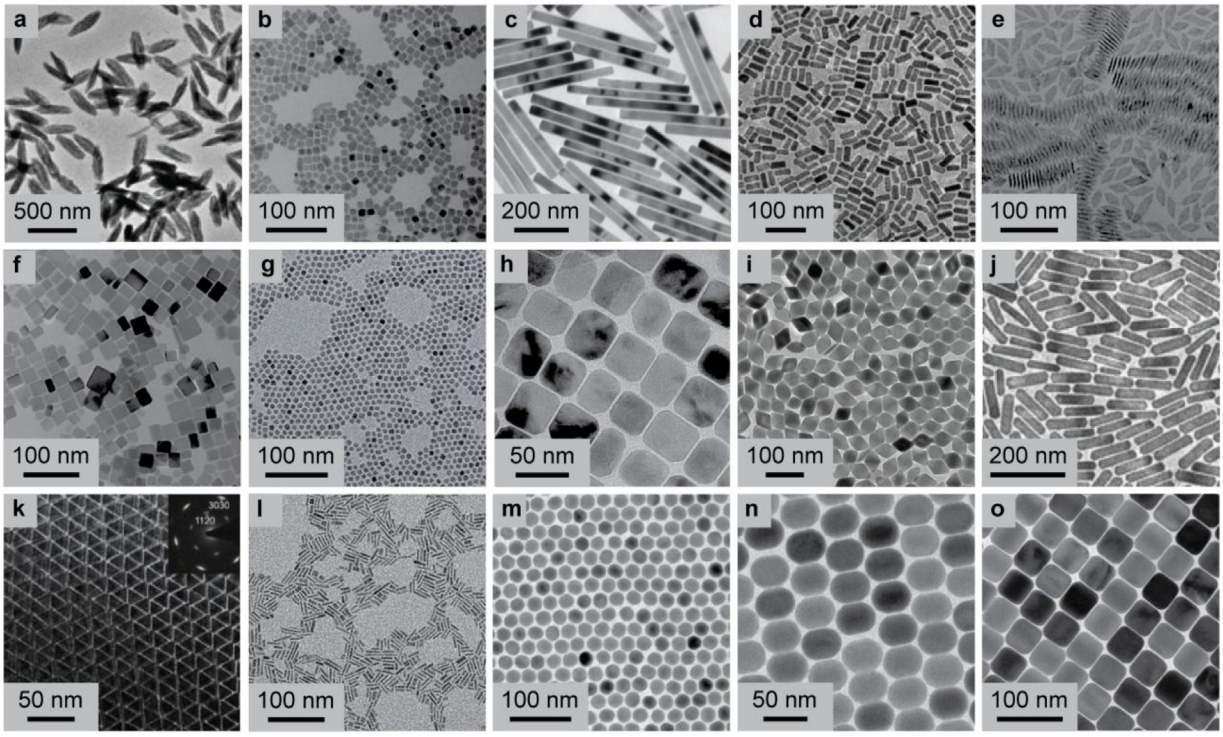

Fig. 2. (a) Typical TEM images of lanthanide-doped (a) YF_3, (b, c) $NaYF_4$ and (d) $NaGdF_4$ nanocrystals synthesized by hydro/solvothermal strategy. (e) GdF_3 nanoparticles prepared through microwave irradiation. (f) $KMnF_3$, (g) CaF_2, (h) $NaScF_4$, (i) $LiYF_4$ and (j) KYb_2F_7 nanoparticles prepared by coprecipitation route. (k) LaF_3, (l) SrF_2 and (m–o) $NaYF_4$ nanoparticles synthesized by thermal decomposition method.
Reproduced with permission from Ref. [60–62,77] (Copyright 2005, 2006, 2007, 2016, American Chemical Society), Ref [17,72]. (Copyright 2010, 2014, Nature Publishing Group), Ref [70,73]. (Copyright 2010, 2011, Wiley-VCH Verlag GmbH & Co. KGaA, Weinheim), Ref. [71,74,76]. (Copyright 2012, 2013, Royal Society of Chemistry), Ref [81]. (Copyright 2010, National Academy of Science, USA), Ref [85]. (Copyright 2010, Springer).

has also been adopted for synthesizing lanthanide-doped LaF_3, $NaYF_4$, $NaScF_4$, $KMnF_3$, $LiYF_4$, KYb_2F_4, SrF_2, $LuPO_4$, and $YbPO_4$ upconversion nanocrystals (Fig. 2f–j) [70–74]. For example, Zhang and colleagues utilized the coprecipitation process to make β-$NaYF_4$:Yb/Er(Tm) nanoparticles in the presence of oleic acid and 1-octadecene [75]. In this work, oleic acid was employed both as a reaction solvent and as a ligand that enables the monodispersity of resulting nanoparticles while 1-octadecene with a high boiling point was used as a primary solvent. By changing the concentration of surfactant, various shapes of $NaYF_4$ nanostructures, such as nanosphere, nanoplate, and nanoellipse, have been selectively synthesized.

Thermal decomposition

Thermal decomposition refers to heat-induced chemical decomposition. It mainly employs an organometallic compound as a precursor, which can decompose into two constituents in a high boiling point organic solvent at elevated temperatures. For the typical synthesis of fluoride-based nanocrystals, metal trifluoroacetate is generally used as a precursor to generate the corresponding metal and fluoride ions [76]. By using this approach, Yan's group first synthesized highly monodisperse LaF_3 nanoparticles [77]. This thermal decomposition method was subsequently adopted for the synthesis of $NaYF_4$-based upconversion nanoparticles by Chow et *al*., who employed oleylamine both as a reaction solvent and as a surface ligand [78]. The advantage of using oleylamine lies in its ability for the synthesis of ultrasmall nanoparticles that are attractive for biological applications. After replacing the oleylamine with oleic acid and 1-octadecene, Capobianco and co-workers reported the controllable synthesis of $NaYF_4$:Yb/Er(Tm) nanocrystals *via* thermal decomposition approach [79,80]. Another significant progress was made by Murray et al., who used thermal decomposition strategy to make highly uniform $NaYF_4$ nanospheres, nanorods, nanoprisms, and nanoplates by controlling the reaction time and the reactant ratio between lanthanide trifluoroacetate and sodium. More interestingly, these as-synthesized nanoparticles can readily assemble and organize into large-size superlattices under appropriate conditions [81]. In addition to fluoride upconversion nanoparticles, Yan's group expanded this approach to the preparation of lanthanide oxides, oxyfluorides, and oxychlorides [82–84].

Manipulation of lanthanide-doped upconversion luminescence

Lanthanide-doped upconversion nanoparticles exhibit excellent luminescent properties. The precise control over the luminescence profiles is of vital importance for their applications in many research fields. To date, a variety of strategies have been developed to manipulate the emission profiles of Ln^{3+}-doped UCNPs. For example, color-tunable emissions can be easily achieved by controlling the combination of dopant-host, particle size, and the concentration of dopants in upconversion nanoparticles [86–88]. However, these approaches generally require stringent modification either on the reaction conditions or the material compositions. Very recently, several complementary methods that offer remote dynamic modulation of upconversion luminescence have been proposed for the lanthanide-doped nanoparticles with a fixed composition. These approaches include the variation of excitation power density and temperature, alteration of excitation pulse width, excitation by sequential pulse pumping, polarization anisotropic modulation, electric field and magnetic field manipulation as well as the applying of mechanical stress [89–95].

In this section, we only highlight the tuning of upconversion emission colors through pulsed laser excitation since other strategies have been well summarized elsewhere. In 2015, Deng et al. reported a non-steady-state upconversion technique to achieve full-color tuning [11]. In their studies, the emission color of Yb/Ho/Ce triply-doped core-shell nanoparticles can be tuned by manipulating the pulsed excitation width of a 980 nm pulsed laser (Fig. 3a). This phenomenon can be understood by considering the dynamic control of energy transfer and the deactivation of the excitation energy during upconversion population process (Fig. 3b). Different from steady-state upconversion excited by a long excitation pulse, only energy levels accessible through fast processed are populated in the presence of a short excitation pulse, resulting in a significant modulation of emission profile upon short-pulse excitation. By pumping with 980 nm pulsed excitation light or with 808 nm continuous-wave laser, the core-shell nanoparticles can emit red, green, and blue fluorescence with tunable intensity ratios (Fig. 3c). The ability to access tunable emission colors allows the achievement of full-color volumetric 3D displays with high spatiotemporal resolution. The combination of pulse width tuning and compositional variability is likely to provide new possibilities for the effective manipulation of Ln^{3+}-doped upconversion luminescence, which is of utmost importance in optical memory, multiplexed imaging, anti-counterfeiting and so on.

Table 2
Current strategies for enhancing photon upconversion in lanthanide-doped nanocrystals. Note that several strategies are employed synergistically in many cases to enhance the upconversion luminescence.

Strategy	Scheme	Ref.
Host Lattice Manipulation	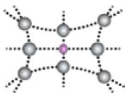	[93,96,97,98,99,100]
Surface Passivation		[19,101,102,103,104,105,106]
Surface Plasmon Coupling	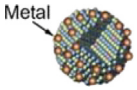	[107,108,109]
Energy Transfer Modulation		[72,112]
Broadband Sensitization	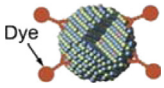	[48,49,50,51,52,53,54,110]
Photonic Crystal Engineering	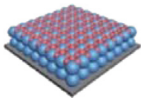	[113,114,115]
Inorganic-organic Hybrid	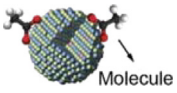	[111]

Enhancement of lanthanide-doped upconversion luminescence

Although promising results have been achieved with the precise control over size, shape, and emission profile of Ln^{3+}-doped UCNPs, the inherent low upconversion efficiency of UCNPs still significantly restricts their practical applications. To date, a range of methods, such as host lattice manipulation, surface passivation, surface plasmon coupling, energy transfer modulation, broadband sensitization, photonic crystals mediation, and inorganic-organic hybrid, have been proposed for optimizing upconversion population and enhancing lanthanide-doped upconversion luminescence, as summarized in Table 2. In this section, we will provide a brief overview of recent advances in enhancing upconversion photoluminescence.

Lanthanide-doped upconversion luminescence mainly originates from intra *f-f* electronic transitions, which can be adjusted by changing the local crystal field. Recent experimental investigations suggest that host lattice manipulation is a simple approach to enhance photon upconversion. For example, owing to large size mismatches between the host cations and dopants, lanthanide acti-

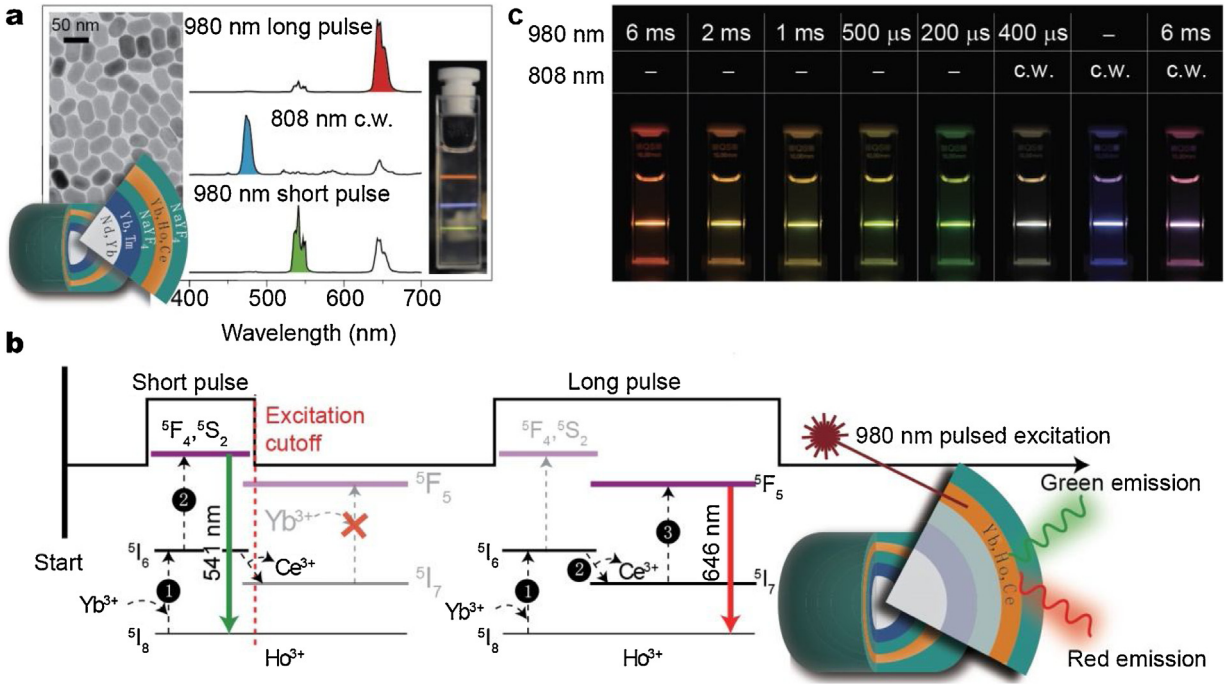

Fig. 3. (a) Rational design and TEM image of $NaYF_4$-based core-shell nanoparticles capable of emitting tunable colors (left inset). Upconversion emission spectra (main panel) and emission photograph (right inset) showing the ability to emit visible RGB color by using the same nanoparticles. (b) Proposed upconversion mechanisms for green/red tuning from an Yb^{3+}–Ho^{3+}–Ce^{3+} triply-doped system through the regulation of pulse width of a 980 nm laser. (c) Luminescence photographs showing multicolor tuning of core-shell sample upon excitation with 808 nm continuous-wave (c.w.) laser and 980 nm pulsed source.
Reproduced with permission from Ref. [11] (Copyright 2015, Nature Publishing Group).

vators' site symmetries is reduced by codoping Li^+, Zn^{2+}, Bi^{3+}, Fe^{3+}, or Sc^{3+} into an upconversion nanoparticle, leading to an enhancement in photon upconversion [96–100]. Besides ion doping, the application of a direct current bias voltage on $BaTiO_3$ host can vary its structural symmetry as well. Using this method, Hao et al. reported the enhancement of green upconversion emission in 2011 [93].

Compared with its bulk counterpart, the upconversion nanoparticle with a high surface-to-volume ratio often suffers from severe surface quenching, resulting in the low upconversion efficiency. Surface passivation through an epitaxial shell coating is an effective strategy to minimize surface quenching effect because all of the lanthanide dopants can be spatially confined in the core region through core-shell design. Until now, several surface passivation strategies, including amorphous shell (non-crystalline silica, carbon) coating, inert shell ($NaYF_4$, $NaGdF_4$) coating, active shell ($NaYF_4$:Yb, $NaGdF_4$:Yb, $BaGdF_5$:Yb) coating, as well as the heterogeneous core-shell structures ($NaYF_4$@$NaGdF_4$, $NaYF_4$@CaF_2, CaF_2@$NaYF_4$), have proven effective in suppressing surface-induced quenching of excitation energy and efficient in enhancing upconversion luminescence [19,101–106].

Surface plasmon coupling is another essential approach to enhancing photon upconversion. It should be noted that the geometric construction of gold and silver greatly influence the peak and band intensity of surface plasmon resonance. By choosing an appropriate metallic structure and optimizing the interaction between metal and UCNPs, researchers have developed many schemes to enhance the luminescence of Ln^{3+}-doped nanoparticles. These hybrid materials not only include the UCNP core decorated with metal nanoparticles, but also refer to UCNP@metal, UCNP@silica@metal, and metal@silica@UCNP multi-layered structures [107–109].

Broadband sensitization has been recently developed as a promising alternative to enhance photon upconversion. Codoping two or more different sensitizers into a nanoparticle can largely expand the excitation region of Ln^{3+}-doped UCNPs. For instance, Wang and co-workers have obtained intense upconversion luminescence, by doping Er^{3+} and Ho^{3+} into a core-shell-shell nanoparticle, upon ultra-broadband excitation [110]. Organic dyes with spectrally broad and intense absorption can be used as broadband sensitizer as well. In a conventional dye-sensitized upconversion system, spectrally broad absorbing dye molecules anchored on the surface of UCNPs can efficiently harvest NIR energy, which is nonradiatively transferred to the sensitizer in the particles, and then sequentially to lanthanide activator for enhanced photon upconversion to proceed [48–54].

Very recently, Zhou et al. reported a phonon-assisted upconversion enhancement at an elevated temperature based on a novel inorganic-organic hybrid system [111]. In their studies, the vibrations of surface-bound molecules through Yb–O chelating can act as surface phonons to promote the energy transfer from Yb^{3+} sensitizers to activators. Although several aspects of this surface phonon-assisted energy transfer remain to be investigated, these hybrid and heterogeneous inorganic-organic systems are highly promising and may find potential applications as nanothermometers in a physiological environment with high resolution. Other notable strategies, including energy transfer modulation, photonic crystal engineering, and super-high-power excitation, have also been proposed and experimentally validated for enhancing photon upconversion [72,112–116].

Emerging applications of lanthanide-doped upconversion nanoparticles

Thanks to the rapid development of well-controlled UCNPs along with their excellent optical properties, researches on Ln^{3+}-doped upconversion nanoparticles have made tremendous progress over the past decade, especially in the area of biomedical applications [21–25]. In addition to the aforementioned advantages of Ln^{3+}-doped UCNPs such as multicolor emission and the absence

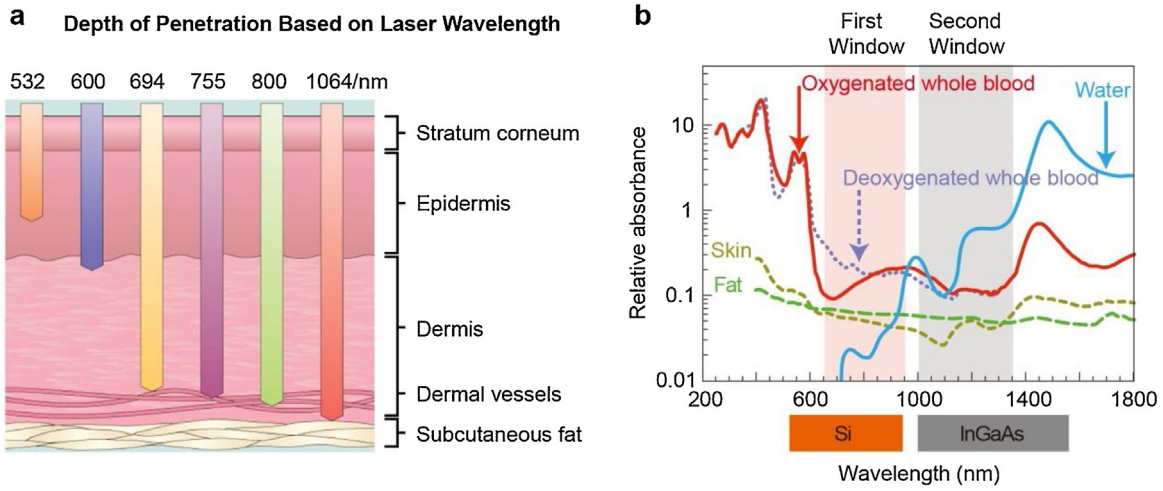

Fig. 4. (a) Wavelength-dependent penetration depths of light into human body tissue. (b) Optical absorption of oxygenated blood, deoxygenated blood, skin, fatty tissue, and water as a function of wavelength. The pink and grey shaded areas indicate the first and second near-infrared windows in biological tissue. Note that silicon (Si) and indium gallium arsenide (InGaAs) cameras are sensitive within the first and second near-infrared windows, respectively.
Reproduced with permission from Ref. [117] (Copyright 2014, Springer) and Ref [118]. (Copyright 2009, Nature Publishing Group).

of autofluorescence in biological specimens, the employment of near-infrared excitation light can also afford a deeper tissue penetration than that of visible light (Fig. 4a) [117]. This is because the currently available excitation sources for photon upconversion are generally within the biological NIR window (650–950 nm), where the absorption and scattering of bio-tissues are minimal (Fig. 4b) [118]. All these characters make Ln^{3+}-doped upconversion nanoparticles ideal candidates for deep tissue imaging, NIR light-activated drug release and therapy [119,120]. However, it should be noted that excitation light at a wavelength of 980 nm can be absorbed by water and thus cause an overheating problem in biological settings. This deleterious effect could be principally alleviated by using Nd^{3+}-sensitized or dye-sensitized nanoparticles upon 800 nm laser excitation because the absorption of water and biological tissues is minimized at this wavelength (Fig. 4b) [46,47].

The employ of Ln^{3+}-doped UCNPs also holds promise for minimizing the transmission losses in photovoltaic devices by translating the sub-bandgap NIR photons into above-bandgap visible ones, which is critical to improving the conversion efficiency of current photovoltaic devices and surpass Shockley–Queisser efficiency limit [121,122]. There are some review papers already published regarding the progress of Ln^{3+}-doped upconversion nanocrystals in the fields of bioscience and photovoltaics [10,25,28,123–126]. Herein, we will give an overview of recent advances in the applications of Ln^{3+}-doped upconversion nanoparticles in some emerging areas. The most recent examples of upconversion nanoparticle-mediated optogenetics, therapeutics, bioimaging, biosensing, super-resolution nanoscopy, remote photoswitching and upconversion lasing are highlighted here.

Upconversion nanoparticle-mediated optogenetics

Optogenetics is a revolutionary biological technique that allows the precise control of activities and functions of neurons by light. Current optogenetic methodologies generally utilize visible light (470/530 nm) to stimulate photo-responsive Channelrhodopsin-2 (ChR2) and halorhodopsin (NpHR) molecules. Despite enormous efforts, the effective activation of targeted neurons by the visible light in deep tissue remains a daunting technical challenge for optogenetic studies in living animals [127–131]. Compared with visible light, NIR irradiation can offer a much greater depth of tissue penetration. Recently, a new class of upconversion-mediated optogenetic system has been developed, by employing Ln^{3+}-doped UCNPs as NIR to the visible transducer, to manipulate the neural activity upon NIR irradiation [132–142].

The concept of upconversion-mediated NIR optogenetic was first demonstrated by Hososhima and co-workers in 2015 [134]. In their studies, $NaYF_4$:Sc/Yb/Er(Tm) upconversion crystals with a size of 100 nm × 500 nm were mixed with collagen to form the neuron culture substrate. When illuminating the specially designed substrate with 975 nm laser, upconversion emissions from $NaYF_4$:Sc/Yb/Er(Tm) particles would activate neurons to induce neuron responses and thus the photocurrent could be observed in the corresponding expressing cells (C1V1 and PsChR). Although high excitation power density required in their experiments can result in overheating problem and false photocurrent signal, this study opens up a promising avenue for controlling neuronal activity in a deep tissue region.

A similar study was later conducted by Shah et al., who used the hybrid scaffolds containing $NaYF_4$:Yb/Tm@$NaYF_4$ upconversion nanoparticles and poly(lactic-co-glycolic acid) as substrate film and investigated the optogenetic control of neuronal activity upon NIR radiation (Fig. 5a) [135]. The blue upconversion luminescence emitted from the core-shell nanoparticles is strong enough to depolarize the ChR2-expressing neurons, leading to a high temporal resolution neuron response. The repetitive action potential at a frequency up to 10 Hz was observed in this work upon pulsed NIR laser excitation. Another recent achievement was demonstrated by Han and co-workers, who realized NIR-induced neuron firing using high-efficient dye-sensitized upconversion nanoparticles [136]. However, considering that dye molecules may undergo photobleaching during continuous NIR laser irradiation, it is uncertain whether dye-sensitized upconversion nanoparticles would outperform ordinary all-inorganic nanoparticles for NIR light-induced neuron activation.

Apart from the *in vitro* studies described above, several interesting results have been achieved in the NIR-mediated *in vivo* deep tissue optogenetics. For example, Zhang et al. reported the activation of ion channel using $NaYF_4$:Yb/Tm upconversion nanoparticles in a *C. elegans* model [137]. The blue emission from the upconversion nanoparticles can drastically change the movement direction of *C. elegans* just like applying a touch force on the worm. However, since *C. elegans* is an optically transparent organism for which blue light can be directly utilized to manipulate neuronal behavior, further investigations are still needed to justify the necessity of upconversion nanoparticles for optogenetic studies in *C. elegans*.

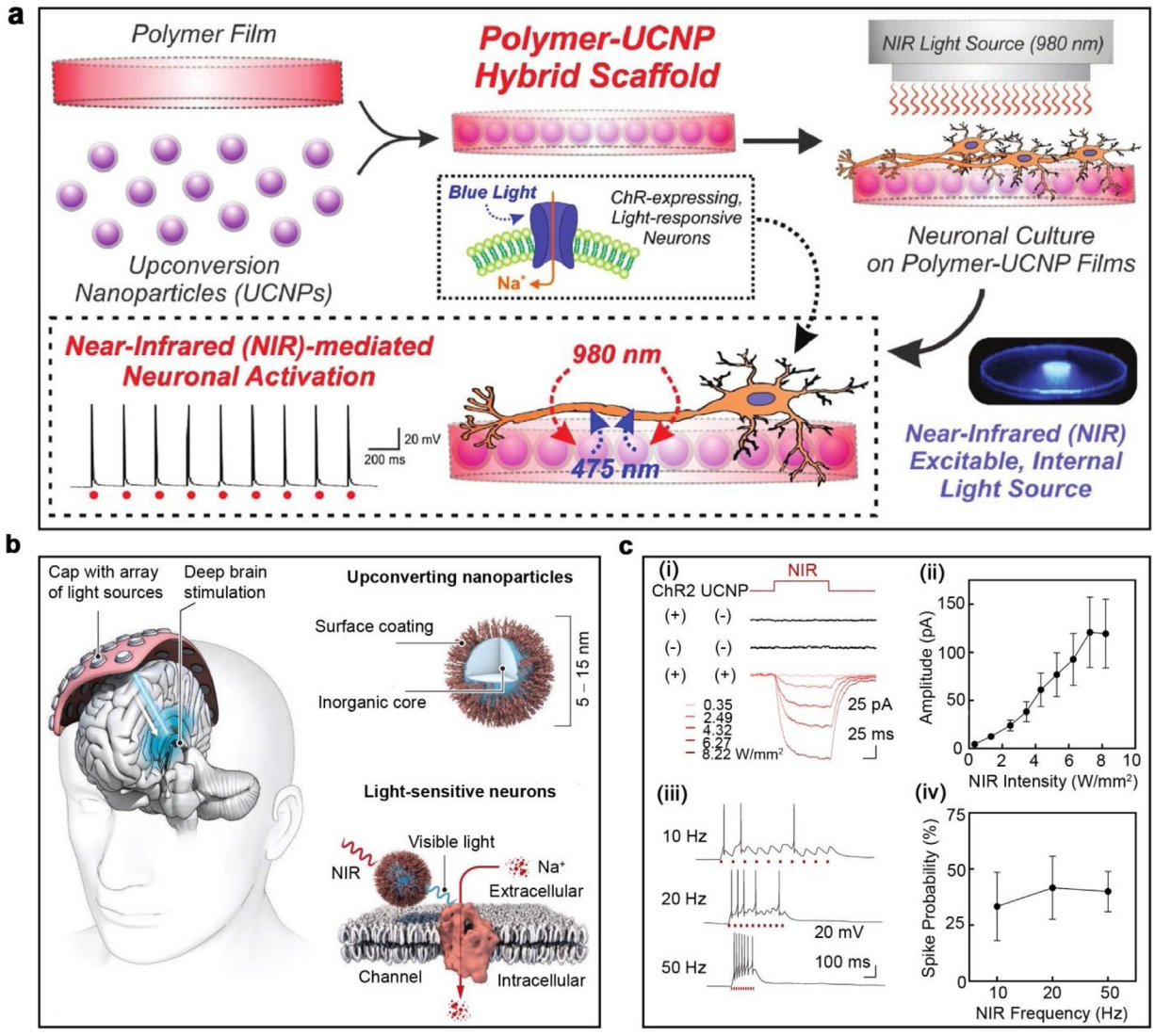

Fig. 5. (a) Rational design of polymer–UCNP hybrid scaffolds for optogenetic neuronal stimulation. The UCNPs served as NIR to blue transducer thus facilitating optogenetic activation of channelrhodopsin (ChR)-expressing neurons upon NIR irradiation. (b) Schematic illumination of NIR deep brain stimulation through upconversion nanoparticles-mediated optogenetics. (c) Characterization of upconversion-based optical stimulation in neurons expressing ChR2. The voltage-clamp and current-clamp traces can be induced in ChR2 neurons using $NaYF_4$:Yb/Tm@SiO_2 upconversion nanoparticles through irradiation with a 980 nm laser.
Reproduced with permission from Ref. [135] (Copyright 2015, Royal Society of Chemistry), Ref [141,142]. (Copyright 2018, Science Publishing Group).

Shi and colleagues have also carried out many research work on upconversion-mediated optogenetics. They firstly verified the feasibility of upconversion nanoparticle-mediated optogenetic modulation of targeted neural circuits in live rodent animals [138]. Subsequently, an all-optical method was developed by them for flexible, wireless neural activity manipulation, including activation and inhibition, in freely moving animals [139,140]. Their studies indicate that Ln^{3+}-doped upconversion nanoparticles can be used for transcranial and deep brain stimulation in awake, freely moving rodents, which is crucial for advanced neural applications.

Very recently, Chen et al. developed an effective method to stimulate specifically labeled neurons in deep brain areas [141]. In their studies, upconverting nanoparticles were injected into the ventral tegmental area (VTA) of the mice brains. Upon NIR irradiation, green or blue luminescence emitted from upconversion nanoparticles could stimulate or inhibit the neuronal activity in deep brain areas (Fig. 5b and c). Using this approach, researchers can stimulate dopamine release through the activation of neurons in the brain, inhibit neuronal activity in the hippocampus, and trigger memory recall by targeting NIR irradiation [142]. This novel strategy might eventually pave the way for clinical treatment of brain diseases, such as Parkinson's and epilepsy.

Upconversion-based cell therapy

Optically triggered cell therapy is one of the most effective approaches for the treatment of medical conditions [143–145]. Photodynamic therapy (PDT) and photothermal therapy (PTT) are two of standard phototherapy methods which have been extensively investigated in recent years [146–152]. Compared with conventional photo-stimulated agents, upconversion-mediated photoactive systems operated in the NIR window can offer deep tissue penetration characteristics [153,154]. Recent progress on upconversion nanoparticles' roles in cellular therapy has demonstrated its viability not only as a stimulator and *in vivo* imaging probe but also, more importantly, as a real-time monitor for cellular treatments.

In a typical upconversion-mediated PDT system, Ln^{3+}-doped UCNPs generally regulate the activation of photosensitizers, which generates reactive oxygen species (ROS) upon NIR irradiation.

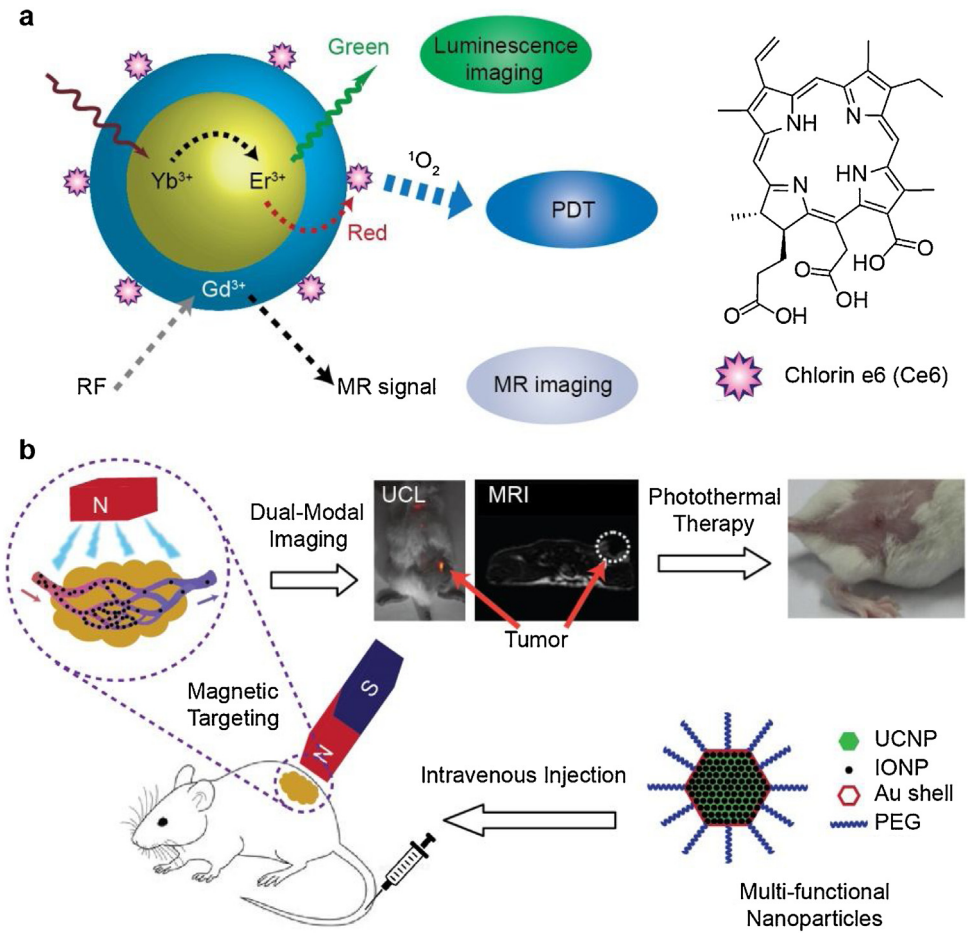

Fig. 6. (a) Schematic illustration of dual-modal imaging and PDT using UCNP-Ce6. Chlorin e6 (Ce6) absorbs red upconversion luminescence and produces singlet oxygen through energy transfer. Another green emission of UCNPs is used for luminescence imaging and shell layer of UCNP doped with Gd^{3+} ion makes magnetic resonance signals for MR imaging. (b) Schematic illustration showing the composition of a multifunctional nanoparticle (MFNP-PEG) and the concept of *in vivo* imaging-guided cancer therapy. The magnetic field around the tumor region induces local tumor accumulation of MFNPs.
Reproduced with permission from Ref. [155] (Copyright 2012, Wiley-VCH Verlag GmbH & Co. KGaA, Weinheim), Ref. [159]. (Copyright 2012, Elsevier B.V.).

Using this strategy, Hyeon and coworkers chose Yb-Er codoped UCNPs and Chlorine e6 (Ce6) as energy donor and photosensitizer, respectively, in their studies. Red upconversion emission from $NaGdF_4$:Yb/Er nanoparticles can be used as an excitation source of Ce6 photosensitizer to induce ROS generation for effective therapy (Fig. 6a) [155].

Despite the rapid development, the non-specific tumor targeting of the upconversion-based agent remains the biggest challenge in nanoparticle-mediated cell therapy. Generally, ROS generated by PDT offers minimal specificities and selectivity, killing both healthy and diseased cells simultaneously. Up to now, many solutions have been reported for overcoming this challenge. For example, by utilizing the folate receptor for active targeting, Zhang et al. developed a highly efficient upconversion-based nanoplatform with specific cancer-targeting abilities for imaging-guided PDT of cancer [156]. Similarly, Tan and coworkers reported upconversion-based PDT using G-quadruplex aptamers for specific targeting and photosensitizer loading. This nanosystem consists of the aptamer for target tracking, G-quadruplex for loading porphyrin-based photosensitizer, and Ln^{3+}-doped UCNPs for imaging and phototherapy, offering high precision in targeting diseased cells [157].

Compared to that of PDT, PTT offers intriguing advantages as more directed phototherapy in cells. Heat-generating optical nanomaterials were capable of producing sufficient localized heating to induce cellular death in specific areas. Li and co-workers reported the use of temperature-feedback upconversion nanoparticles combined with photothermal material for real-time monitoring of microscopic temperature in PTT. Upon NIR excitation, the microscopic temperature of photothermal material is high enough to kill cancer cells while keeping the temperature of lesions low enough to protect healthy tissue from damage [158]. Another representative advance was reported by Liu et al. in 2011. In their studies, an upconversion-based multifunctional nanoplatform was developed for imaging-guided and magnetic-targeted optical cancer therapy. More importantly, the integration of metal nanocomplexes with magnetic responsive elements allows for enhanced photothermal, imaging and targeting efficacy (Fig. 6b) [159]. Although nanoparticle therapeutics is regarded as an emerging treatment modality for cancer [160–162], potential problems such as *in vivo* bio-stability of these nanoparticles are still yet to be resolved.

3D cellular imaging through upconversion

Fluorescence cellular imaging is one of the most direct tools innovated for understanding cellular dynamics. While advanced fluorescence imaging techniques have been developed over the years, there are still fundamental challenges in distinguishing intracellular activities in 2D imaging. In contrast, 3D imaging of living cells can provide a more detailed and accurate spatial visualization of the interplay of cells and their components than achieveable by conventional 2D imaging systems, in which the imaging process often leads to artifactual observations [163–165].

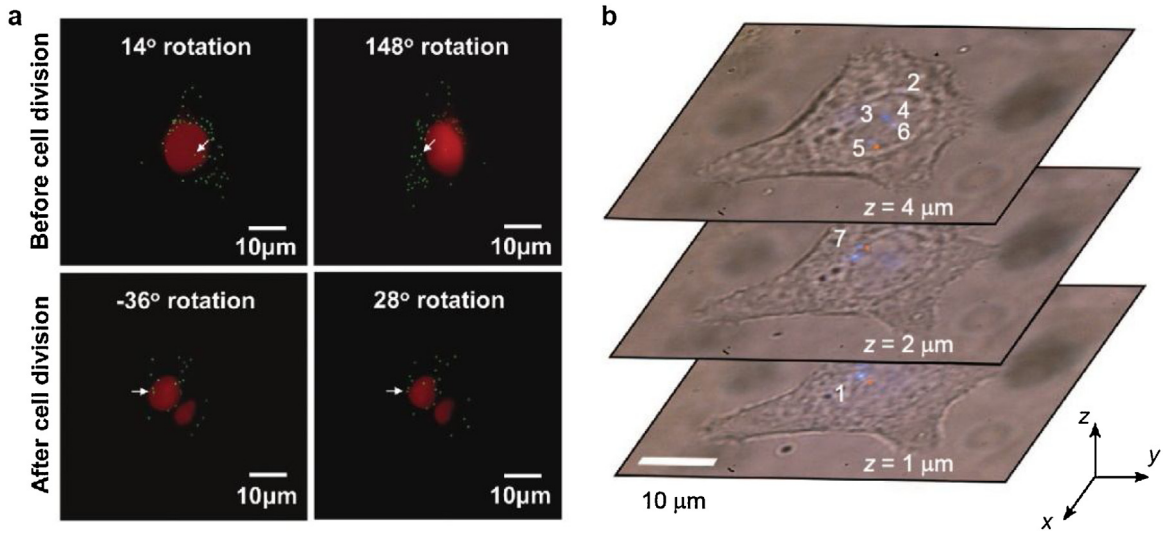

Fig. 7. (a) Wide-field 3D cell imaging of upconversion nanoparticles (green) internalized in HeLa cells, whose nuclei were conjugated to red fluorescent protein (red). The nuclei and Ln^{3+}-doped UCNPs were imaged upon excitation at 532 nm and 980 nm, respectively. The reconstructed 3D images of live cells viewed from different angles before (top) and after (bottom) the division. (b) Wide-field upconversion fluorescence microscopy method for determining single nanoparticles long-term 3D tracking. Three representative single-cell images containing seven nanoparticle spots at different heights (1, 2 and 4 μm) are recorded by a CCD camera.
Reproduced with permission from Ref. [175] (Copyright 2015, Royal Society of Chemistry), Ref [179]. (Copyright 2018, Nature Publishing Group).

Resolving the molecular mechanisms in living cells by single-particle tracking methods has allowed many molecular behaviors to be deciphered [166–169]. Accompanying the advancements in intracellular particle tracking, the interactions between cells and nanoparticle, especially quantum dots (QDs), have been studied extensively. The multicolor characteristics offered by QDs have advantages over conventional probes, allowing multiplex readout signals and ease of surface modification to facilitate 3D cellular imaging [170–172]. However, the heavy metal ion-induced cytotoxicity and photoblinking characteristic restricted their practical application in biological systems [173]. As a replacement, Ln^{3+}-doped UCNPs offer minimal cytotoxicity and excellent optical stability for bio-imaging. In addition, the usage of upconversion nanoparticles as imaging probes could enable 3D imaging through conventional confocal microscopy techniques [174]. All these merits make Ln^{3+}-doped UCNPs ideal probe for 3D imaging with high contrast even in wide-field microscopy systems. For example, Lee and coworkers combined the wide-field NIR excitation and step motor for 3D single upconversion nanoparticle localization (Fig. 7a). In this study, upconversion nanoparticles were excited with NIR light, leading to the elimination of blurred out-of-focus signals and the creation of 3D images with high locational precision. This upconversion-based imaging probe offers sufficient accuracies for imaging reconstruction, with a positional accuracy of about 4 nm on the *xy* axes and 15 nm on the *z*-axis. [175].

Despite numerous reports, *z*-axis motion in intracellular particle tracking is still a severe problem [176–178]. Upconversion-guided 3D imaging can offer unprecedented solutions for precision in determining locational information of single particles even with wide-field excitation for optimal long-term particle tracking. For instance, Jin and coworkers reported 3D high-resolved single upconversion nanoparticle tracking through intensity-based analysis. Their approach was conducted by separating the optical data of single particle from those of nanoclusters, which allowed for single-cell imaging with nanoparticles located at different heights of 1, 2 and 4 μm (Fig. 7b). By tracking a single nanoparticle with high temporal, spectral and spatial resolution, the measurement of local viscosity in intracellular environment was implemented as well [179].

Biosensor

Fluorescence-based biosensor, which enables active fluorescence qualitative and quantitative analysis, has been commonly used in various fields due to their high sensitivity and ease of manufacturing [180–183]. Ln^{3+}-doped UCNPs with zero autofluorescence characteristics are one of the most suitable systems for fluorescence-based assay [184–187]. One interesting example of upconversion-based bio-detecting platforms is in the form of a pH sensor, where the variation of pH could be measured through the ratiometric changes in upconversion emission from different bands [188,189]. By using this method, Schäferling and coworkers performed intracellular pH sensing [190]. In their studies, the pH indicator (pHrodo) conjugated on the surface of nanoparticles was sensitized *via* an energy transfer from Ln^{3+}-doped UCNPs, and the change of pH was detected through the comparison of emission intensity between upconversion nanoparticles (550 nm) and pH-sensitive pHrodo dye (590 nm) (Fig. 8a). These upconversion-based probes provide a suitable solution for detecting the changes of pH both *in vitro* and *in vivo* models with high biological background fluorescence.

Similar to optical pH sensing, upconversion-based nanothermometer is capable of measuring localized temperatures through ratiometric changes in different emission bands [191–195]. A representative example was best exemplified by Capobianco et al. in the year of 2010, who determined the temperature of a single cell using the upconversion-based optical method. In this work, the upconversion emission intensity ratio between $^2H_{11/2} \rightarrow {}^4I_{15/2}$ (525 nm) and $^4S_{3/2} \rightarrow {}^4I_{15/2}$ (545 nm) transitions of Er^{3+} ions was exploited to sense the changes of temperature (Fig. 8b) [196]. More interestingly, by incubating the upconversion nanoparticles with HeLa cells, this upconversion-based fluorescent nanothermometer can measure the internal temperature of the living cell from 25 °C to 45 °C, which is vitally important for understanding its pathology and physiology.

Upconversion-based biosensors also have emerging abilities for the detection of specific chemicals in living systems [197–199]. For example, Zhu and coworkers designed a noncoding RNA sensing nanoplatform through the DNA hybridization between DNA-modified upconversion nanoparticles and gold nanoparticles

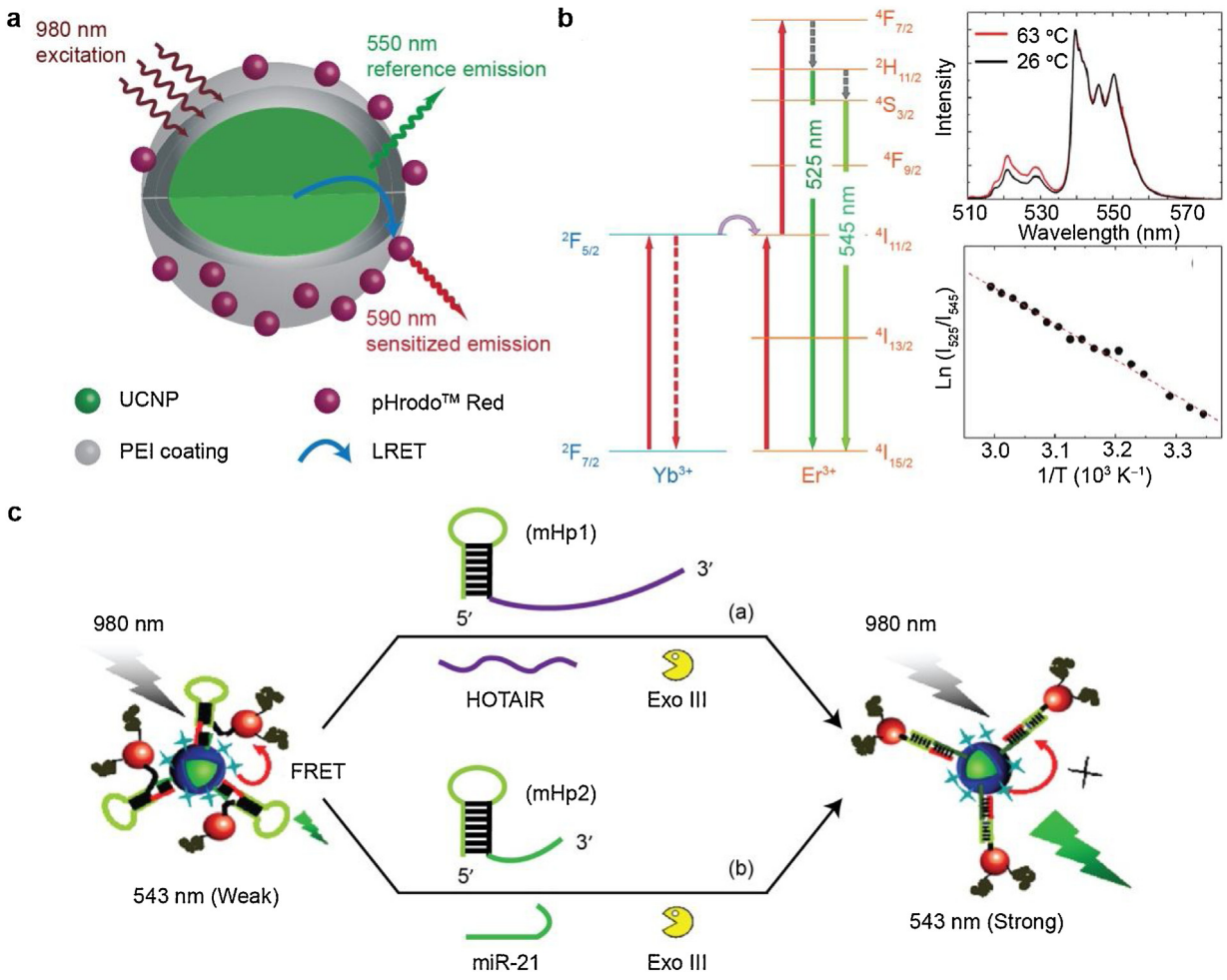

Fig. 8. (a) Schematic illustration of upconversion-based pH sensor. The pHrodo dye can be sensitized *via* an energy transfer from the nanoparticle. By comparing the emission intensity between upconversion nanoparticles (550 nm) and pH-sensitive pHrodo dye (590 nm), the pH can be measured. (b) The intensity ratio of green upconversion emission bands from $^2H_{11/2} \rightarrow {}^4I_{15/2}$ and $^4S_{3/2} \rightarrow {}^4I_{15/2}$ transitions of Er^{3+} ions is employed to detecting temperature through optical method. (c) Schematic illustration of the established sensing nanoplatform for detecting (a) antisense RNA segment and (b) miRNA. The hairpin sequence was designed to respond toward a specific target DNA. In the presence of single DNA, the hairpin is open and the Au nanoparticles move away from the surface of UCNPs, resulting in the recovery of upconversion luminescence emitted at 543 nm.
Reproduced with permission from Ref. [190] (Copyright 2017, American Chemical Society), Ref [196]. (Copyright 2010, American Chemical Society), Ref [200]. (Copyright 2018, Wiley-VCH Verlag GmbH & Co. KGaA, Weinheim).

[200]. In their studies, the quenching of upconversion emission *via* fluorescence resonance energy transfer can be recovered by designing a signal DNA sequence to open the hairpin DNA. In addition, an exonuclease III (Exo III)-assisted cycling amplification strategy was introduced to improve the sensing sensitivity (Fig. 8c). All these characteristics make upconversion-based sensing platform potential candidates for various ncRNA detection and clinical diagnosis.

Stimulated emission depletion (STED) nanoscopy

Another important area for applications of upconversion nanoparticles is their use for super-resolution imaging. Stimulated emission depletion (STED) micro/nanoscopy is one of the most important techniques for achieving sub-diffraction-limit super-resolution imaging [201–204]. However, the current STED micro/nanoscopy approaches generally using organic dyes as the probe and requiring extremely high power depletion laser, which will quickly cause the photobleaching of dye molecules and the deterioration of imaging capability [205–207]. As an alternative, Ln^{3+}-doped UCNPs with inherent non-photobleaching and non-photoblinking properties could be selected as luminescent probes for STED imaging to enable long term and repetitive imaging with high temporal resolution [208–211]. In addition, compared with single-photon emission STED, upconversion-based multiphoton STED is more suitable for deep tissue studies since the scattering from biotissues is much less significant in the NIR region.

The first example of optical depletion of lanthanides' upconversion was demonstrated by Zhan and co-workers [208]. In their studies, green emission of $NaYF_4$:Yb^{3+}/Er^{3+} upconversion nanoparticles, arising from laser excitation at 795 nm, could be depleted by introducing 1140 nm laser as another pumping source. Although the depletion efficiency is low, this work indicates that Ln^{3+}-doped UCNPs are potential probes for sub-diffraction microscopic imaging.

Very recently, Jin and colleagues have reported a new approach to realize low-power super-resolution STED nanoscopy (Fig. 9a) [210]. Upconversion nanoparticles with high concentration (8 mol%) Tm^{3+} dopant are used as luminescent probes. In comparison to the luminescence of $NaYF_4$:Yb/Tm (20/1 mol%) nanocrystals, the blue emission of Tm^{3+} upon 980 nm excitation could be largely counteracted in the $NaYF_4$:Yb/Tm (20/8 mol%) nanoparticles once another de-excitation beam at 808 nm was applied (Fig. 9b). A photon-avalanche-like effect and a depletion route of $^3H_4 \rightarrow {}^3H_6$ were proposed to explain the concentration-dependent stimulated

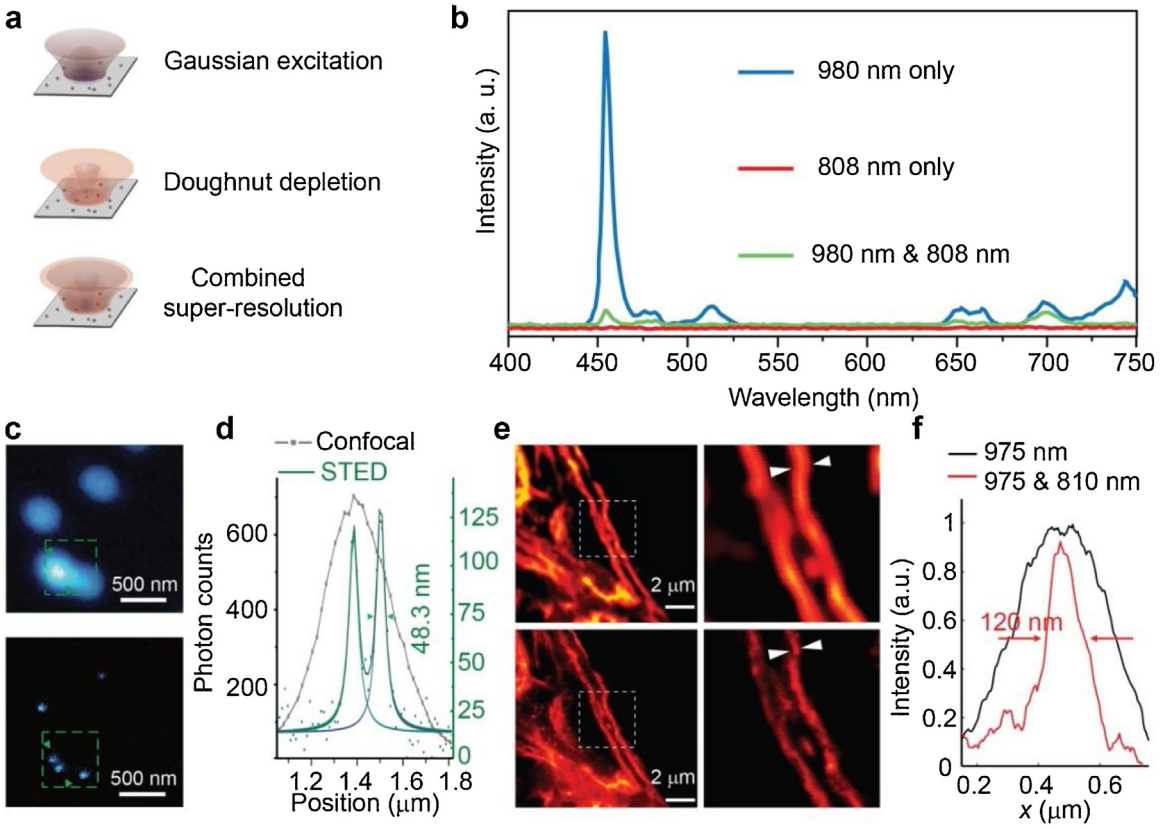

Fig. 9. (a) Schematic diagram of upconversion-based STED super-resolution imaging. Note that a Gaussian excitation at 980 nm and a 'doughnut' depletion at 808 nm are employed for STED nanoscopy. (b) Upconversion emission spectra of $NaYF_4$:Yb/Tm (20/8 mol%) upconversion nanoparticles upon 980 nm, 808 nm and dual excitations. (c) Respective confocal (upper) and upconversion-STED super-resolution (bottom) images. (d) The corresponding line profiles analyses showing a full width at half maximum (FWHM) of 48.3 nm by using the upconversion-STED method. (e) Multiphoton (upper) and upconversion-STED super-resolution (bottom) images of cytoskeleton protein desmin using secondary antibody conjugated $NaYF_4$:Yb/Tm (18/10 mol%) upconversion nanoparticles and the corresponding intensity profiles analyses (f). Reproduced with permission from Ref. [210,211] (Copyright 2017, Nature Publishing Group).

emission depletion phenomenon. More importantly, the 808 nm doughnut-shaped depletion beam at a relatively low power density (9.75 MW/cm^2) could dim the overlapping area, resulting in the size of a luminescence spot far below the diffraction limit (Figs. 9c and d). This smart design not only enables super-resolution imaging at high lateral resolutions but also inhibits the photothermal damage induced by a high-power laser beam.

Almost at the same time, Zhan et al. also demonstrated the feasibility of STED by employing upconversion nanoparticles with heavily doped Tm^{3+} ions [211]. The optical depletion mechanism is similar to the above mentioned, although a different depletion channel ($^1D_2 \rightarrow {}^3F_2$) was proposed in their work. Using this low-power super-resolution STED nanoscopy method, a resolution of 66 nm was achieved upon dual NIR irradiation at 975 nm and 810 nm. By mixing $NaYF_4$:Yb/Tm (18/10 mol%) and $NaGdF_4$:Yb/Tm (40/10 mol%)@$NaGdF_4$:Tb (15 mol%) nanoparticles as luminescent probes, a two-color super-resolution imaging was obtained experimentally. Moreover, this upconversion-based STED nanoscopy can be used to image subcellular structures with a high later imaging resolution (Figs. 9e and f). Although these results are promising, the application of inorganic upconversion nanocrystals as labels for STED nanoscopy is in its infancy compared to organic fluorophores. There are still many issues that need to be addressed before applying it in real biological systems.

NIR light-activated molecular switches

Conventional molecular switches generally require the use of UV and visible light to induce photochemical reactions between two isomers with different structures (Fig. 10a), which may cause deleterious effects associated with low storage density for optical memory and low penetration depth for photo-release and photodynamic therapy [212–216]. Ln^{3+}-doped upconversion nanoparticles, with their unique NIR to UV–vis emission property, provide a possible solution to these problems. By employing UCNP as an antenna, upconversion-based photoswitching systems have been proven to be capable of reversible modulation of properties and structures of photoswitchable molecules, such as spiropyrans, diarylethenes, and azobenzenes [217–221].

In 2009, Branda et al. demonstrated an interesting structural switching of photo-responsive dithienylethene (DTE) molecules using upconversion-mediated technology [222]. In their studies, a mixture of upconversion nanoparticles and DTE molecules was cast into the acrylate film. Upon irradiation with 980 nm laser, ultraviolet emission from $NaYF_4$:Yb/Tm and green luminescence from $NaYF_4$:Yb/Er particles can be produced to trigger ring-opening and ring-closing reactions of the DTE molecules, respectively. One year later, a two-way reversible photoswitching relied on one type of nanoparticle was reported by the same group, where $NaYF_4$:Yb/Tm@$NaYF_4$:Yb/Er@$NaYF_4$ nanoparticles are used as energy donor upon NIR irradiation [223]. At a high-power density, the dominant UV emissions arise from Tm^{3+} can drive a ring-closing reaction of DTE molecule. In contrast, a low power density leads to a ring-opening reaction of the organic molecule, as a result of green emission from Er^{3+}. Based on a similar method, Li and co-workers demonstrated a reversible tuning of self-organized helical superstructures by doping chiral switch molecules and upconversion nanoparticles into a liquid crystal host

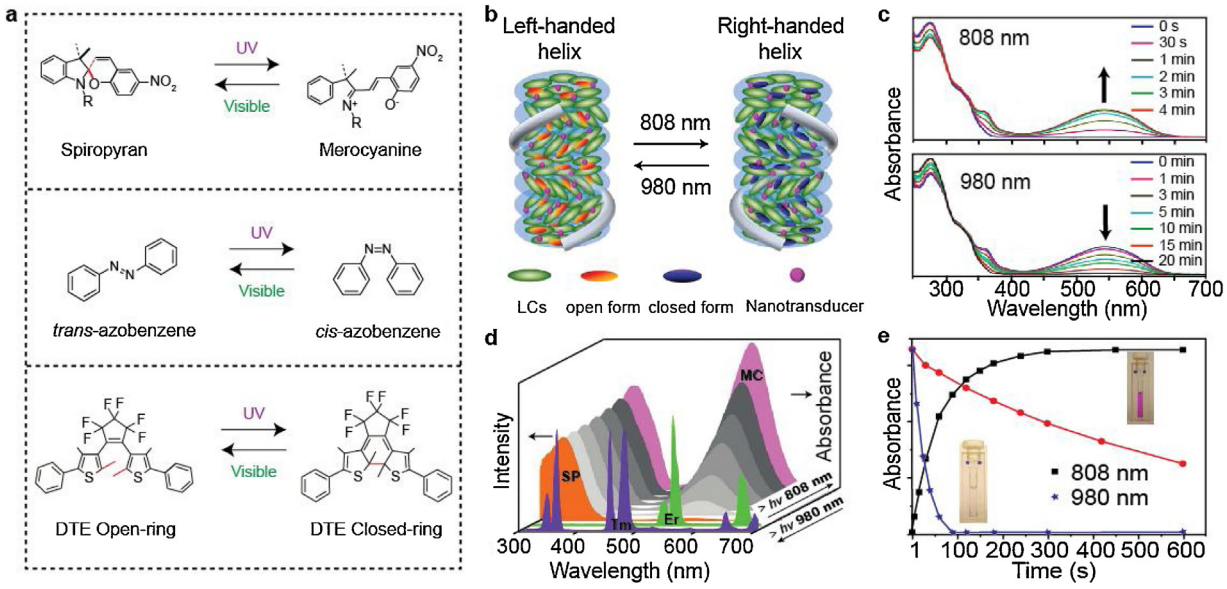

Fig. 10. (a) Typical examples of photochromic molecules. Note that UV and visible light are commonly used for activating photoisomerization reaction of these photochromic molecules. (b) Schematic diagram of dual NIR-light triggered reversible handedness inversion of the self-organized helical superstructure incorporated with chiral diarylethene switch and upconversion nanotransducers. (c) Time-dependent UV–Vis spectra changes of molecule switch (*S, S*)-**8** mixed with upconversion nanoparticles in cyclohexane upon 808 nm laser irradiation (top spectra) and the reverse process under 980 nm laser excitation (bottom spectra). (d) Upconversion emissions from Tm^{3+} (purple spectrum) and Er^{3+} (green spectrum) with the excitation at 808 nm and 980 nm, respectively, which overlap well with the absorption spectra of SP and MC. The evolution of the UV–vis spectra of SP and MC molecules upon NIR irradiation is shown as well. (e) Kinetic monitoring of absorbance changes of MC molecule at 560 nm in the presence of the core-shell upconversion nanoparticles (black square: upon 808 nm irradiation; blue star: upon 980 nm irradiation). The red dots show the absorbance changes of MC in the dark. Reproduced with permission from Ref. [225,226] (Copyright 2014 and 2015, Wiley-VCH Verlag GmbH & Co. KGaA, Weinheim).

[224]. Upon laser irradiation at 980 nm, a power density-dependent reversible switching process was observed accompany with the shift of reflection wavelength of the photonic superstructure. Interestingly, a reversible dynamic tuning of RGB reflections in a single film is implemented by simply adjusting the power densities of NIR excitation laser. Despite the enticing prospect, the spectral overlap of UV and visible emissions of these upconversion transducers compromises the photochemical reaction rate and reaction degree.

As an alternative, upconversion nanoparticles with the orthogonal excitation-emission property have been developed and utilized for inducing NIR light-activated photoswitching. For example, Li and colleagues have demonstrated a reversible photocyclization of the chiral diarylethene molecular through dual-channel upconversion (Fig. 10b) [225]. Upon 808 nm irradiation, the UV emission of Tm^{3+} facilitated the structural transformation of DTE molecule from the open to the closed form, as accompanied by an absorption change of DTE at 550 nm. Similarly, the reverse ring-opening reaction could be achieved using a 980 nm laser irradiation (Fig. 10c). Another representative demonstration of orthogonal upconversion-driven photoswitching was reported by Lee et al. [226]. In their studies, the ultraviolet emission from Tm^{3+} upon 808 nm excitation and visible emission from Er^{3+} under 980 nm irradiation can trigger structural transmission between spiropyran (SP) and merocyanine (MC) along with the solution color change between pink and colorless (Fig. 10d and e). Owing to the unique NIR light-activated switching characteristic, these spiropyran-modified upconversion nanoparticles may find important applications in photoswitchable drug release and photodynamic therapy in deep tissue. Recently, Liu and co-workers developed a new type of orthogonal excitation-emission upconversion nanoparticles with ultra-high spectral purity. By combining these upconversion nanoparticles with diarylethene photochromic molecules, optical data writing and erasing are easily implemented through laser excitation at 980 nm and 1532 nm, respectively [227]. This NIR light-based two-way molecular editing opens up a multifaceted approach for rewritable optical memory with high spatiotemporal resolution.

Upconversion lasing

Lanthanide-doped upconversion nanoparticles can also be employed as efficient optical gain media for lasing applications. Yu and colleagues have devoted many efforts in this field and reported several interesting phenomena associated with upconversion lasing. In 2013, they demonstrated the first upconversion multi-band lasing by utilizing $NaYF_4$:Yb/Er@$NaYF_4$ nanoparticles as gain media [228]. In their studies, a 980 nm 3-pulse pumping system was used as the excitation source. By building an upconversion nanoparticle-contained Fabry-Perot cavity and employing sequential pulses excitation, amplified spontaneous emission from Er^{3+} ions was achieved through the increase of pumping power. More excitingly, whispering gallery mode (WGM) upconversion lasing emissions from blue, green, and red bands of Er^{3+} ions were generated from a bottle-like microcavity, which is fabricated by coating a drop of hybrid silica resin onto a bare optical fiber (Fig. 11a). Three years later, Wang et al. reported the deep ultraviolet upconversion lasing emission from $NaYF_4$@$NaYbF_4$:Tm/Gd@$NaYF_4$ upconversion nanoparticles using the similar bottle-structured microresonator through the optimization of pumping scheme [229]. The 5-pulse excitation scheme used in this work was proven to be favorable for pumping the multiphoton upconversion (Fig. 11b). With increasing the pumping energy, two typical threshold powers, P_a and P_{th}, were presented in the *S*-liked light input-output curve (Fig. 11c), which is a typical characteristic for lasing emission. The high *Q* factor (~2800) and well-defined sharp peaks (linewidth < 0.11 nm) indicated a high quality of ultraviolet upconversion lasing (Fig. 11d).

In addition to bottle-like microcavities, there are many other structures that have proven effective for generating upconversion lasing. For example, Yu and co-workers have developed a cylindrical microcavity containing $NaYF_4$:Yb,Tm@$NaYF_4$ nanocrystals to induce upconversion lasing through 5-pulse system pumping

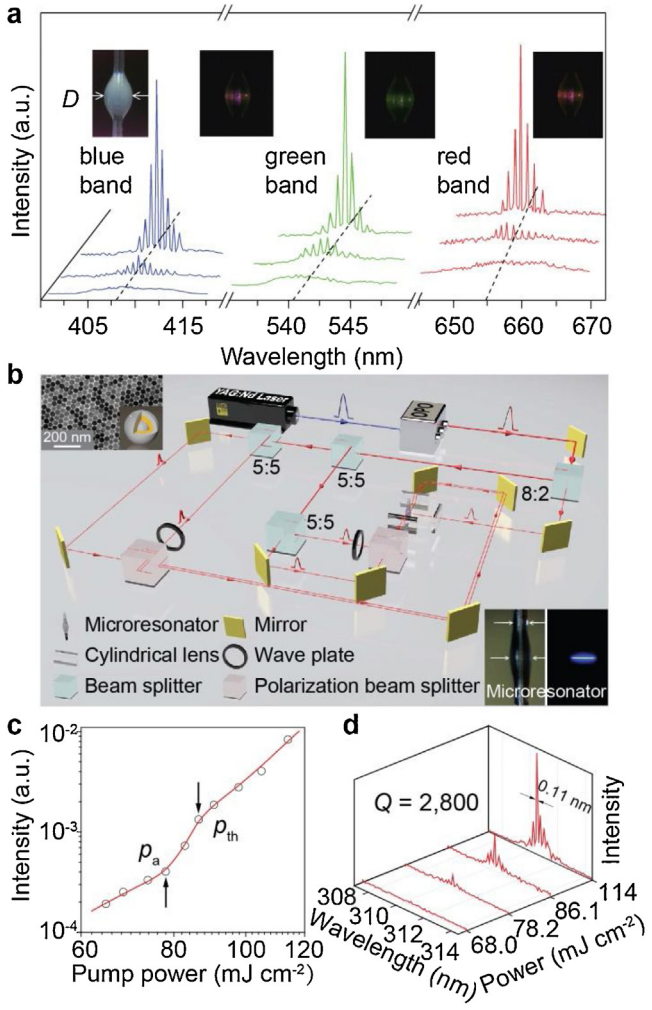

Fig. 11. (a) Power-dependent lasing spectra of the microcavity containing $NaYF_4$:Yb/Er@$NaYF_4$ nanoparticles. The insets present the bottle-like geometry of microcavity under daylight and the images of the microcavity under different excitation power. (b) Schematic of the optical set-up of the five-pulse excitation scheme for upconversion lasing. The insets show TEM image of $NaYF_4$@$NaYbF_4$:Tm@$NaYF_4$ upconversion nanoparticles (upper left) and photographs of the microresonator without and with laser excitation (lower right). (c) Log-log plot of output intensity versus pumping power of a microresonator containing upconversion nanoparticles. This *S*-like spectrum indicates a transition from spontaneous emission to an amplified spontaneous emission and a lasing emission. (d) The lasing spectra of Gd^{3+} ions at different excitation power.
Reproduced with permission from Ref. [228] (Copyright 2013, American Chemical Society), Ref [229]. (Copyright 2016 Nature Publishing Group).

[230]. The deleterious recombination of the intermediate excited states can be suppressed through the integration of cylindrical microcavity, leading to multiphoton upconversion enhanced and lasing emissions from Tm^{3+} ions occurred. Another white-light WGM upconversion lasing has been successfully obtained in Yb-Er-Tm codoped $NaYF_4$ hexagonal microrods through total internal reflection within the six flat inner-surfaces of hexagonal prisms [231,232]. Moreover, besides the lasing emissions from lanthanides' intra 4*f* electronic transitions, UV upconversion lasing of Ce^{3+} ions from their 5*d*-4*f* transition has also been demonstrated by Wang's group using $NaYbF_4$:Gd/Tm@$NaGdF_4$@CaF_2:Ce upconversion nanoparticles as gain medium [233]. Finally, in addition to high-energy pulse excitation source, continuous-wave pumping laser also can be used to generate lasing emission. Very recently, continuous-wave upconverted lasing has been reported employing $NaYF_4$:Gd/Tm@$NaGdF_4$ nanoparticles as gain media. By coupling Tm^{3+}-doped upconversion nanoparticles to the surface of 5 μm polystyrene microspheres, Schuck et al. developed a upconverting microlaser through c.w. laser excitation at 1064 nm with power density as low as 14 kW cm^{-2}. Due to the energy-looping excitation property of $NaYF_4$:Gd/Tm@$NaGdF_4$ nanoparticles, lasing threshold can be reduced remarkably, leading to the stable operation of this microlaser upon excitation with 300 kW cm^{-2} for 5 h [234]. These newly developed upconversion-based lasers open up a new avenue toward applications in biosensing and deep-tissue optogenetics.

Conclusions and outlook

Lanthanide-doped upconversion nanoparticles have received increasing attention in recent years because of their unique NIR excitation characteristics and exceptional light penetration depth, along with sharp emission bands, large anti-Stokes shifts, and remarkable photostability. In this review, we have summarized recent development of lanthanide-doped upconversion nanocrystals mainly focusing on controllable synthesis, multicolor emission tuning, luminescence enhancement, and especially the emerging applications from nanobiology to nanophotonics.

Despite the exceptional promise of Ln^{3+}-doped UCNPs, there remain several challenges in this field. A major restriction is their low quantum efficiency, particularly under low power density excitation. Recently, dye-sensitized upconversion has been proposed to achieve luminescence enhancement in lanthanide-doped nanocrystals. However, the underlying mechanisms in these hybrid systems need to be clarified and explained further. Another area in need of development is the standard measuring facilities and protocols for characterizing the quantum efficiency of upconversion nanoparticles. Owing to the typical excitation power dependence of upconversion efficiency, a criterion on the measurement of quantum yield is highly required to make a quantitative comparison between different samples from different laboratories.

For application in neuroscience, upconversion nanoparticles can be readily taken up by cells, resulting in the distance variation between membrane-bound ion channels and the particles, which in turn restrains the long-term stimulation with high stability. For the case of upconversion-based STED, there are also many issues when it applied in real biological tissues under physiological conditions, such as long imaging acquisition time and limited spatial resolution caused by particle size. All these issues must be well addressed before upconversion nanoparticles can indeed find their practical utility.

Acknowledgements

This work is supported by the Singapore Ministry of Education (Grant MOE2017-T2-2-11), Agency for Science, Technology and Research (Grant A1883c0011), National Research Foundation, Prime Minister's Office, Singapore under the NRF Investigatorship programme its Competitive Research Program (CRP Award No. NRF-NRFI05-2019-0003), National Natural Science Foundation of China (11774133, 21771135, and 61705137), and the Science and Technology Project of Shenzhen (JCYJ20170817093821657, KQJSCX20180328093614762). Y.D.S. was supported by KRICT (KK1933-10, SKO1930-20), the Global Research Laboratory (GRL) Program through the National Research Foundation of Korea (NRF) (no. 2016911815), and the Bio Industrial Strategic Technology Development Program (no. 10077582) funded by the Ministry of Trade, Industry & Energy (MOTIE, Korea).

References

[1] F. Auzel, Chem. Rev. 104 (2004) 139–174.
[2] V.V. Ovsyakin, P.P. Feofilov, JETP Lett. Engl. 4 (1966) 317–318.
[3] F. Auzel, Phys. Rev. B: Solid State 13 (1976) 2809–2817.

[4] M. Pollnau, D.R. Gamelin, S.R. Lüthi, H.U. Güdel, M.P. Hehlen, Phys. Rev. B 61 (2000) 3337–3346.
[5] D. Matsuura, Appl. Phys. Lett. 81 (2002) 4526–4528.
[6] G.K. Liu, Chem. Soc. Rev. 44 (2015) 1635–1652.
[7] J.F. Suyver, J. Grimm, M.K. van Veen, D. Biner, K. Krämer, H.U. Güdel, J. Lumin. 117 (2006) 1–2.
[8] G. K. Liu, B. Jacquier, Springer Berlin/Heidelberg New York (2005).
[9] J. Zhou, Q. Liu, W. Feng, Y. Sun, F.Y. Li, Chem. Rev. 115 (2015) 395–465.
[10] X.Y. Huang, S.Y. Han, W. Huang, X.G. Liu, Chem. Soc. Rev. 42 (2013) 173–201.
[11] R.R. Deng, F. Qin, R.F. Chen, W. Huang, M.H. Hong, X.G. Liu, Nat. Nanotechnol. 10 (2015) 237–242.
[12] B. Zhou, B.Y. Shi, D.Y. Jin, X.G. Liu, Nat. Nanotechnol. 10 (2015) 924–936.
[13] Y.H. Wang, J. Ohwaki, Appl. Phys. Lett. 63 (1993) 3268–3270.
[14] R.H. Page, K.I. Schaffers, P.A. Waide, J.B. Tassano, S.A. Payne, W.F. Krupke, W.K. Bischel, J. Opt. Soc. Am. B 15 (1998) 996–1008.
[15] N. Rakov, C.B. de Araújo, Y. Messaddeq, M.A. Aegerter, Appl. Phys. Lett. 70 (1997) 3084–3086.
[16] S. Heer, K. Kömpe, H.U. Güdel, M. Haase, Adv. Mater. 16 (2004) 2102–2105.
[17] F. Wang, Y. Han, C.S. Lim, Y.H. Lu, J. Wang, J. Xu, H.Y. Chen, C. Zhang, M.H. Hong, X.G. Liu, Nature 463 (2010) 1061–1065.
[18] Z.Q. Li, Y. Zhang, S. Jiang, Adv. Mater. 20 (2008) 4765–4769.
[19] G.S. Yi, G.M. Chow, Chem. Mater. 19 (2007) 341–343.
[20] A. Patra, C.S. Friend, R. Kapoor, P.N. Prasad, J. Phys. Chem. B 106 (2002) 1909–1912.
[21] X.Z. Ai, C.J.H. Ho, J.X. Am, A.B.E. Attia, J. Mu, Y. Wang, X.Y. Wang, Y. Wang, X.G. Liu, H.B. Chen, M.Y. Gao, X.Y. Chen, E.K.L. Yeow, G. Liu, M. Olivo, B.G. Xing, Nat. Commun. 7 (2016) 10432.
[22] J. Zhao, J.H. Gao, W.T. Xue, Z.H. Di, H. Xing, Y. Lu, L.L. Li, J. Am. Chem. Soc. 140 (2018) 578–581.
[23] H. Dong, S.R. Du, X.Y. Zhang, G.M. Lyu, L.D. Sun, L.D. Li, P.Z. Zhang, C. Zhang, C.H. Yan, Chem. Rev. 115 (2015) 10725–10815.
[24] D.K. Chatterjee, A.J. Rufaihah, Y. Zhang, Biomaterials 29 (2008) 937–943.
[25] J. Zhou, Z. Liu, F.Y. Li, Chem. Soc. Rev. 41 (2012) 1323–1349.
[26] J.C. Boyer, F.C.J.M. van Veggel, Nanoscale 2 (2010) 1417–1419.
[27] D.O. Faulkner, S. Petrov, D.D. Perovic, N.P. Kherani, G.A. Ozin, J. Mater. Chem. 22 (2012) 24330–24334.
[28] G.Y. Chen, H.L. Qiu, P.N. Prasad, X.Y. Chen, Chem. Rev. 114 (2014) 5161–5214.
[29] Q.S. Chen, X.J. Xie, B.L. Huang, L.L. Liang, S.Y. Han, Z.G. Yi, Y. Wang, Y. Li, D.Y. Fan, L. Huang, X.G. Liu, Angew. Chem. Int. Ed. 56 (2017) 7605–7609.
[30] X. Wang, A. Yakovliev, T.Y. Ohulchanskyy, L.N. Wu, S.J. Zeng, X.J. Han, J.L. Qu, G.Y. Chen,Adv. Opt. Mater. 6 (2018), 1800690.
[31] L. Liu, S.F. Wang, B.Z. Zhao, P. Pei, Y. Fan, X.M. Li, F. Zhang, Angew. Chem. Int. Ed. 57 (2018) 7518–7522.
[32] T.Y. Sun, Y.H. Li, W.L. Ho, Q. Zhou, X. Chen, J.M. Li, H.M. Zhu, B.L. Huang, J. Lin, E. Brent, S.T. Chu, F. Wang, Nat. Commun. 10 (2019) 1811.
[33] L.Y. Wang, Y.D. Li, Chem. Commun. (2006) 2557–2559.
[34] K.W. Krämer, D. Biner, G. Frei, H.U. Güdel, M.P. Hehlen, S.R. Lüthi, Chem. Mater. 16 (2004) 1244–1251.
[35] E. De la Rosa, P. Salas, H. Desirena, C. Angeles, R.A. Rodríguez,Appl. Phys. Lett. 87 (2005), 241912.
[36] W.P. Qin, Z.Y. Liu, C.N. Sin, C.F. Wu, G.S. Qin, Z. Chen, K.Z. Zheng, Light Sci. Appl. 3 (2014) e193.
[37] H.J. Liang, G.Y. Chen, L. Li, Y. Liu, F. Qin, Z.G. Zhang, Opt. Commun. 282 (2009) 3028–3031.
[38] Y. Dwivedi, S.N. Thakur, S.B. Rai, Appl. Phys. B: Laser Opt. 89 (2007) 45–51.
[39] D.Q. Chen, L. Liu, P. Huang, M.Y. Ding, J.S. Zhong, Z.G. Ji, J. Phys. Chem. Lett. 6 (2015) 2833–2840.
[40] J.S. Chivian, W.E. Case, D.D. Eden, Appl. Phys. Lett. 35 (1979) 124–125.
[41] F. Wang, R.R. Deng, J. Wang, Q.X. Wang, Y. Han, H.M. Zhu, X.Y. Chen, X.G. Liu, Nat. Mater. 10 (2011) 968–973.
[42] H.L. Wen, H. Zhu, X. Chen, T.F. Hung, B.L. Wang, G.Y. Zhu, S.F. Yu, F. Wang, Angew. Chem. Int. Ed. 52 (2013) 13419–13423.
[43] F. Shi, J.S. Wang, X.S. Zhai, D. Zhao, W.P. Qin, CrystEngComm 13 (2011) 3782–3787.
[44] P. Huang, W. Zheng, S. Zhou, D. Tu, Z. Chen, H. Zhu, R. Li, E. Ma, M. Huang, X. Chen, Angew. Chem. Int. Ed. 53 (2014) 1252–1257.
[45] G.C. Pan, X. Bai, D.W. Yang, X. Chen, P.T. Jing, S.N. Qu, L.J. Zhang, D.L. Zhou, J.Y. Zhu, B. Dong, H.W. Song, Nano Lett. 17 (2017) 8005–8011.
[46] H. Dong, L.D. Sun, C.H. Yan, Chem. Soc. Rev. 44 (2015) 1608–1634.
[47] X.J. Xie, Z.J. Li, Y.W. Zhang, S.H. Guo, A.I. Pendharkar, M. Lu, L. Huang, W. Huang, G. Han,Small 13 (2017), 1602843.
[48] W.Q. Zou, C. Visser, J.A. Maduro, M.S. Pshenichnikov, J.C. Hummelen, Nat. Photonics 6 (2012) 560–564.
[49] G.Y. Chen, J. Damasco, H.L. Qiu, W. Shao, T.Y. Ohulchanskyy, R.R. Valiev, X. Wu, G. Han, Y. Wang, C.H. Yang, H. Ågren, P.N. Prasad, Nano Lett. 15 (2015) 7400–7407.
[50] X. Wu, H. Lee, O. Bilsel, Y.W. Zhang, Z.J. Li, T. Chen, Y. Liu, C.Y. Duan, J. Shen, A. Punjabi, G. Han, Nanoscale 7 (2015) 18424–18428.
[51] G.Y. Chen, W. Shao, R.R. Valiev, T.Y. Ohulchanskyy, G.S. He, H. Ågren, P.N. Prasad, Adv. Opt. Mater. 4 (2016) 1760–1766.
[52] J.T. Xu, P.P. Yang, M.D. Sun, H.T. Bi, B. Liu, D. Yang, S.L. Gai, F. He, J. Lin, ACS Nano 11 (2017) 4133–4144.
[53] S.W. Hao, Y.F. Shang, D.Y. Li, H. Ågren, C.H. Yang, G.Y. Chen, Nanoscale 9 (2017) 6711–6715.
[54] D.J. Garfield, N.J. Borys, S.M. Hamed, N.A. Torquato, C.A. Tajon, B.N. Tian, B. Shevitski, E.S. Barnard, Y.D. Suh, S. Aloni, J.B. Neaton, E.M. Chan, B.E. Cohen, P.J. Schuck, Nat. Photonics 12 (2018) 402–407.
[55] X.Y. Li, X.W. Liu, D.M. Chevrier, X. Qin, X.J. Xie, S.Y. Song, H.J. Zhang, P. Zhang, X.G. Liu, Angew. Chem. Int. Ed. 54 (2015) 13312–13317.
[56] T. Aidilibike, J.J. Guo, L.L. Wang, X.H. Liu, Y.Y. Li, W.P. Qin, RSC Adv. 7 (2017) 2676–2681.
[57] T. Aidilibike, Y.Y. Li, J.J. Guo, X.H. Liu, W.P. Qin, J. Mater. Chem. C 4 (2016) 2123–2126.
[58] X.H. Liu, T. Aidilibike, J.J. Guo, Y.Y. Li, W.H. Di, W.P. Qin, RSC Adv. 7 (2017) 14010–14014.
[59] X. Wang, J. Zhuang, Q. Peng, Y.D. Li, Nature 437 (2005) 121–124.
[60] X. Wang, J. Zhuang, Q. Peng, Y.D. Li, Inorg. Chem. 45 (2006) 6661–6665.
[61] L.Y. Wang, Y.D. Li, Chem. Mater. 19 (2007) 727–734.
[62] J.F. Ren, G.H. Jia, Y.Y. Guo, A.X. Wang, S.Q. Xu, J. Phys. Chem. C 120 (2016) 1342–1351.
[63] F. Zhang, Y. Wang, T. Yu, F.Q. Zhang, Y.F. Shi, S.H. Xie, Y.G. Li, L. Xu, B. Tu, D.Y. Zhao, Angew. Chem. Int. Ed. 46 (2007) 7976–7979.
[64] D.Q. Chen, Y.L. Yu, F. Huang, P. Huang, A.P. Yang, Y.S. Wang, J. Am. Chem. Soc. 132 (2010) 9976–9978.
[65] D.Q. Chen, Y.L. Yu, F. Huang, Y.S. Wang, Chem. Commun. 47 (2011) 2601–2603.
[66] T.D. Nguyen, C.T. Dinh, T.O. Do, ACS Nano 4 (2010) 2263–2273.
[67] S. Heer, O. Lehmann, M. Haase, H.U. Güdel, Angew. Chem. Int. Ed. 42 (2003) 3179–3182.
[68] J.W. Stouwdam, F.C.J.M. van Veggel, Nano Lett. 2 (2002) 733–737.
[69] G.S. Yi, G.M. Chow, J. Mater. Chem. 15 (2005) 4460–4464.
[70] J. Wang, F. Wang, C. Wang, Z. Liu, X.G. Liu, Angew. Chem. Int. Ed. 50 (2011) 10369–10372.
[71] Y. Ai, D.T. Tu, W. Zheng, Y.S. Liu, J.T. Kong, P. Hu, Z. Chen, M.D. Huang, X.Y. Chen, Nanoscale 5 (2013) 6430–6438.
[72] J. Wang, R.R. Deng, M.A. MacDonald, B.L. Chen, J.K. Yuan, F. Wang, D.Z. Chi, T.S. Andy Hor, P. Zhang, G.K. Liu, Y. Han, X.G. Liu, Nat. Mater. 13 (2014) 157–162.
[73] W. Zheng, S.Y. Zhou, Z. Chen, P. Hu, Y.S. Liu, D.T. Tu, H.M. Zhu, R.F. Li, M.D. Huang, X.Y. Chen, Angew. Chem. Int. Ed. 52 (2013) 6671–6676.
[74] Y.X. Zhang, P. Hu, D. Wang, J.C. Chen, W.Z. Liu, P. Hu, M.D. Huang, X.Y. Chen, Z. Chen, Nanoscale 10 (2018) 15485–15495.
[75] Z.Q. Li, Y. Zhang,Nanotechnology 19 (2008), 345606.
[76] D.Q. Chen, Y.L. Yu, F. Huang, H. Lin, P. Huang, A.P. Yang, Z.X. Wang, Y.S. Wang, J. Mater. Chem. 22 (2012) 2632–2640.
[77] Y.W. Zhang, X. Sun, R. Si, L.P. You, C.H. Yan, J. Am. Chem. Soc. 127 (2005) 3260–3261.
[78] G.S. Yi, G.M. Chow, Adv. Funct. Mater. 16 (2006) 2324–2329.
[79] J.C. Boyer, L.A. Cuccia, J.A. Capobianco, Nano Lett. 7 (2007) 847–852.
[80] J.C. Boyer, F. Vetrone, L.A. Cuccia, J.A. Capobianco, J. Am. Chem. Soc. 128 (2006) 7444–7445.
[81] X.C. Ye, J.E. Collins, Y.J. Kang, J. Chen, D.T.N. Chen, A.G. Yodh, C.B. Murray, Proc. Natl. Acad. Sci. U. S. A. 107 (2010) 22430–22435.
[82] R. Si, Y.W. Zhang, L.P. You, C.H. Yan, Angew. Chem. Int. Ed. 44 (2005) 3256–3260.
[83] Y.P. Du, Y.W. Zhang, Z.G. Yan, L.D. Sun, C.H. Yan, J. Am. Chem. Soc. 131 (2009) 16364–16365.
[84] Y.P. Du, Y.W. Zhang, L.D. Sun, C.H. Yan, J. Am. Chem. Soc. 131 (2009) 3162–3163.
[85] H.Q. Wang, T. Nann, Nanoscale Res. Lett. 6 (2011) 267.
[86] S.Y. Han, X. Qin, Z.F. An, Y.H. Zhu, L.L. Liang, Y. Han, W. Huang, X.G. Liu, Nat. Commun. 7 (2016) 13059.
[87] F. Vetrone, J.C. Boyer, J.A. Capobianco, A. Speghini, M. Bettinelli, J. Appl. Phys. 96 (2004) 661–667.
[88] D.Q. Chen, L. Lei, J. Xu, A.P. Yang, Y.S. Wang,Nanotechnology 24 (2013), 085708.
[89] B. Chen, Y. Liu, Y. Xiao, X. Chen, Y. Li, M.Y. Li, X.S. Qiao, X.P. Fan, F. Wang, J. Phys. Chem. Lett. 7 (2016) 4916–4921.
[90] D.D. Li, Q.Y. Shao, Y. Dong, J.Q. Jiang, J. Phys. Chem. C 118 (2014) 22807–22813.
[91] Y.D. Han, H.Y. Li, Y.B. Wang, Y. Pan, L. Huang, F. Song, W. Huang, Sci. Rep. 7 (2017) 1320.
[92] P. Rodríguez-Sevilla, Y.H. Zhang, N. de Sousa, M.I. Marqués, F. Sanz-Rodríguze, D. Jaque, X.G. Liu, P. Haro-González, Nano Lett. 16 (2016) 8005–8014.
[93] J.H. Hao, Y. Zhang, X.H. Wei, Angew. Chem. Int. Ed. 50 (2011) 6876–6880.
[94] Y.X. Liu, D.S. Wang, J.X. Shi, Q. Peng, Y.D. Li, Angew. Chem. Int. Ed. 52 (2013) 4366–4369.
[95] M.D. Wisser, M. Chea, Y. Lin, D.M. Wu, W.L. Mao, A. Salleo, J.A. Dionne, Nano Lett. 15 (2015) 1891–1897.
[96] G.Y. Chen, H.C. Liu, H.J. Liang, G. Somesfalean, Z.G. Zhang, J. Phys. Chem. C 112 (2008) 12030–12036.
[97] H.J. Liang, Y.D. Zheng, G.Y. Chen, L. Wu, Z.G. Zhang, W.W. Cao, J. Alloys Compd. 509 (2011) 409–413.
[98] N. Niu, F. He, S.L. Gai, C.X. Li, X. Zhang, S.H. Huang, P.P. Yang, J. Mater. Chem. 22 (2012) 21613–21623.
[99] P. Ramasamy, P. Chandra, S.W. Rhee, J. Kim, Nanoscale 5 (2013) 8711–8717.
[100] Q.M. Huang, J.C. Yu, E. Ma, K.M. Lin, J. Phys. Chem. C 114 (2010) 4719–4724.
[101] Q. Lü, F.Y. Guo, L. Sun, A.H. Li, L.C. Zhao,J. Appl. Phys. 103 (2008), 123533.

[102] F. Vetrone, R. Naccache, V. Mahalingam, C.G. Morgan, J.A. Capobianco, Adv. Funct. Mater. 19 (2009) 2924–2929.
[103] Y.F. Wang, L.D. Sun, J.W. Xiao, W. Feng, J.C. Zhou, J. Shen, C.H. Yan, Chem. Eur. J. 18 (2012) 5558–5564.
[104] J. Zuo, D.P. Sun, L.P. Tu, Y.N. Wu, Y.H. Cao, B. Xue, Y.L. Zhang, Y.L. Chang, X.M. Liu, X.G. Kong, W.J. Buma, E.J. Meijer, H. Zhang, Angew. Chem. Int. Ed. 57 (2017) 3054–3058.
[105] H. Rabie, Y.X. ng, N. Pasquale, M.J. Lagos, P.E. Batson, K.B. Lee,Adv. Mater. 31 (2019), 1970104.
[106] Q. Liu, Y.X. Zhang, C.S. Peng, T.S. Yang, L.M. Joubert, S. Chu, Nat. Photonics 12 (2018) 548–553.
[107] L. Sudheendra, V. Ortalan, S. Dey, N.D. Browning, I.M. Kennedy, Chem. Mater. 23 (2011) 2978–2993.
[108] W. Deng, L. Sudheendra, J.B. Zhao, J.X. Fu, D.Y. Jin, I.M. Kennedy, E.M. Goldys,Nanotechnology 22 (2011), 325604.
[109] F. Zhang, G.B. Braun, Y.F. Shi, Y.C. Zhang, X.H. Sun, N.O. Reich, D.Y. Zhao, G. Stucky, J. Am. Chem. Soc. 132 (2010) 2850–2851.
[110] D.Q. Chen, L. Lei, A.P. Yang, Z.X. Wang, Y.S. Wang, Chem. Commun. 48 (2012) 5898–5900.
[111] J.J. Zhou, S.H. Wen, J.Y. Liao, C. Clarke, S.A. Tawfik, W. Ren, C. Mi, F. Wang, D.Y. Jin, Nat. Photonics 12 (2018) 154–158.
[112] G. Tian, Z.J. Gu, L.J. Zhou, W.Y. Yin, X.X. Liu, L. Yan, S. Jin, W.L. Ren, G.M. Xing, S.J. Li, Y.L. Zhao, Adv. Mater. 24 (2012) 1226–1231.
[113] W.B. Niu, L.T. Su, R. Chen, Y. Wang, A. Palaniappan, H.D. Sun, A.I.Y. Tok, Nanoscale 6 (2014) 817–824.
[114] Z. Yin, H. Li, W. Xu, S.B. Cui, D.L. Zhou, X. Chen, Y.S. Zhu, G.S. Qin, H.W. Song, Adv. Mater. 28 (2016) 2518–2525.
[115] C.L.M. Hofmann, E.H. Eriksen, S. Fischer, B.S. Richards, P. Balling, J.C. Goldschmidt, Opt. Express 26 (2018) 7537–7554.
[116] J.B. Zhao, D.Y. Jin, E.P. Schartner, Y.Q. Lu, Y.J. Liu, A.V. Zvyagin, L.X. Zhang, J.M. Dawes, P. Xi, J.A. Piper, E.M. Goldys, T.M. Monro, Nat. Nanotechnol. 8 (2013) 729–734.
[117] Arne A. Meesters, Luiza H.U. Pitassi, Valeria Campos, Albert Wolkerstorfer, Christine C. Dierickx, Laser Med. Sci. 29 (2014) 481–492.
[118] A.M. Smith, M.C. Mancini, S.M. Nie, Nat. Nanotechnol. 4 (2009) 710–711.
[119] J. Xu, L.G. Xu, C.Y. Wang, R. Yang, Q. Zhuang, X. Han, Z.L. Dong, W.W. Zhu, R. Peng, Z. Liu, ACS Nano 11 (2017) 4463–4474.
[120] L. Rao, L.L. Bu, B. Cai, J.H. Xu, A. Li, W.F. Zhang, Z.J. Sun, S.S. Guo, W. Liu, T.H. Wang, Adv. Mater. 28 (2016) 3460–3466.
[121] G.E. Arnaoutakis, J. Marques-Hueso, A. Ivaturi, S. Fischer, J.C. Goldschmidt, K.W. Krämer, B.S. Richards, Sol. Energy Mater. Sol. Cells 140 (2015) 217–223.
[122] K.V. Krishnaiah, P. Venkatalakshmamma, C. Basavapoornima, I.R. Martin, K. Soler-Carracedo, M.A. Hernandez-Rodriguez, V. Venkatramu, C.K. Jayasankar, Mater. Chem. Phys. 199 (2017) 67–72.
[123] A. Gnach, A. Bednarkiewicz, Nano Today 7 (2012) 532–563.
[124] G.Y. Chen, I. Roy, C.H. Yang, P.N. Prasad, Chem. Rev. 116 (2016) 2826–2885.
[125] W. Zheng, P. Huang, D.T. Tu, E. Ma, H.M. Zhu, X.Y. Chen, Chem. Soc. Rev. 44 (2015) 1379–1415.
[126] S.L. Gai, C.X. Li, P.P. Yang, J. Lin, Chem. Rev. 114 (2014) 2343–2389.
[127] K. Deisseroth, Nat. Methods 8 (2011) 26–29.
[128] G. Nagel, T. Szellas, W. Huhn, S. Kateriya, N. Adeishvili, P. Berthold, D. Ollig, P. Hegemann, E. Bamberg, Proc. Natl. Acad. Sci. U. S. A. 100 (2003) 13940–13945.
[129] E.S. Boyden, F. Zhang, E. Bamberg, G. Nagel, K. Deisseroth, Nat. Neurosci. 8 (2005) 1263–1268.
[130] K. Deisseroth, Nat. Neurosci. 18 (2015) 1213–1225.
[131] O. Yizhar, L.E. Fenno, M. Prigge, F. Schneider, T.J. Davidson, D.J. O'Shea, V.S. Sohal, I. Goshen, J. Finkelstein, J.T. Paz, K. Stehfest, R. Fudim, C. Ramakrishnan, J.R. Huguenard, P. Hegemann, K. Deisseroth, Nature 477 (2011) 171–178.
[132] L. He, Y.W. Zhang, G.L. Ma, P. Tan, Z.J. Li, S.B. Zang, X. Wu, J. Jing, S.H. Fang, L.J. Zhou, Y.J. Wang, Y. Huang, P.G. Hogan, G. Han, Y.B. Zhou, eLife 4 (2015) e10024.
[133] A. Pliss, T.Y. Ohulchanskyy, G.Y. Chen, J. Damasco, C.E. Bass, P.N. Prasad, ACS Photonics 4 (2017) 806–814.
[134] S. Hososhima, H. Yuasa, T. Ishizuka, M.R. Hoque, T. Yamashita, A. Yamanaka, E. Sugano, H. Tomita, H. Yawo, Sci. Rep. 5 (2015) 16533.
[135] S. Shah, J.J. Liu, N. Pasquale, J. Lai, H. McGowan, Z.P. Pang, K.B. Lee, Nanoscale 7 (2015) 16571–16577.
[136] X. Wu, Y. Zhang, K. Takle, O. Bilsel, Z. Li, H. Lee, Z. Zhang, D. Li, W. Fan, C. Duan, E.M. Chan, C. Lois, Y. Xiang, G. Han, ACS Nano 10 (2016) 1060–1066.
[137] A. Bansal, H. Liu, M.K. Jayakumar, S. Andersson-Engels, Y. Zhang, Small 12 (2016) 1732–1743.
[138] X.D. Lin, Y. Wang, X. Chen, R.H. Yang, Z.X. Wang, J.Y. Feng, H.T. Wang, K.W.C. Lai, J.F. He, F. Wang, P. Shi,Adv. Healthc. Mater. 6 (2017), 1700446.
[139] Y. Wang, X.D. Lin, X. Chen, X. Chen, Z. Xu, W.C. Zhang, Q.H. Liao, X. Duan, X. Wang, M. Liu, F. Wang, J.F. He, P. Shi, Biomaterials 142 (2017) 136–148.
[140] X.D. Lin, X. Chen, W.C. Zhang, T.Y. Sun, P.L. Fang, Q.H. Liao, X. Chen, J.F. He, M. Liu, F. Wang, P. Shi, Nano Lett. 18 (2018) 948–956.
[141] S. Chen, A.A. Weitemier, X. Zeng, L.M. He, Y.Y. Wang, Y.Q. Tao, A.J.Y. Huang, Y. Hashimotodani, M. Kano, H. Iwasaki, L.K. Parajuli, S. Okabe, D.B. Loong Teh, Angelo H. All, I. Tsutsui-Kimura, K.F. Tanaka, X.G. Liu, T.J. McHugh, Science 359 (2018) 679–684.
[142] N. Feliu, E. Neher, W.J. Parak, Science 359 (2018) 633–634.
[143] D.E.J.G.J. Dolmans, D. Fukumura, R.K. Jain, Nat. Rev. Cancer 3 (2003) 380–387.
[144] T.J. Dougherty, C.J. Gomer, B.W. Henderson, G. Jori, D. Kessel, M. Korbelik, J. Moan, Q. Peng, J. Natl. Cancer Inst. Monographs 90 (1998) 889–905.
[145] Y.C. Pan, J.J. Yang, X.W. Luan, X.L. Liu, X.Q. Li, J. Yang, T. Huang, L. Sun, Y.Z. Wang, Y.H. Lin, Y.J. Song, Sci. Adv. 5 (2019) eaav7199.
[146] I. Roy, T.Y. Ohulchanskyy, H.E. Pudavar, E.J. Bergey, A.R. Oseroff, J. Morgan, T.J. Dougherty, P.N. Prasad, J. Am. Chem. Soc. 125 (2003) 7860–7865.
[147] B.B. Ding, S. Shao, C. Yu, B. Teng, M.F. Wang, Z.Y. Cheng, K.L. Wong, P.A. Ma, J. Lin,Adv. Mater. 30 (2018), 1802479.
[148] N.M. Idris, M.K. Gnanasammandhan, J. Zhang, P.C. Ho, R. Mahendran, Y. Zhang, Nat. Med. 18 (2012) 1580–1585.
[149] Z.Y. Hou, Y.X. Zhang, K.R. Deng, Y.Y. Chen, X.J. Li, X.R. Deng, Z.Y. Cheng, H.Z. Lian, C.X. Li, J. Lin, ACS Nano 9 (2015) 2584–2599.
[150] X.F. Yan, G. Niu, J. Lin, A.J. Jin, H. Hu, Y.X. Tang, Y.J. Zhang, A.G. Wu, J. Lu, S.L. Zhang, P. Huang, B.Z. Shen, X.Y. Chen, Biomaterials 42 (2015) 94–102.
[151] K. Yang, G.B. Yang, L. Chen, L. Cheng, L. Wang, C.C. Ge, Z. Liu, Biomaterials 38 (2015) 1–9.
[152] W.W. Li, P.F. Rong, K. Yang, P. Huang, K. Sun, X.Y. Chen, Biomaterials 45 (2015) 18–26.
[153] M. Nyk, R. Kumar, T.Y. Ohulchanskyy, E.J. Bergey, P.N. Prasad, Nano Lett. 8 (2008) 3834–3838.
[154] Y.I. Park, K.T. Lee, Y.D. Suh, T. Hyeon, Chem. Soc. Rev. 44 (2015) 1302–1317.
[155] Y.I. Park, H.M. Kim, J.H. Kim, K.C. Moon, B. Yoo, K.T. Lee, N. Lee, Y. Choi, W. Park, D. Ling, K. Na, W.K. Moon, S.H. Choi, H.S. Park, S.Y. Yoon, Y.D. Suh, S.H. Lee, T. Hyeon, Adv. Mater. 24 (2012) 5755–5761.
[156] X.M. Liu, M. Zheng, X.G. Kong, Y.L. Zhang, Q.H. Zeng, Z.C. Sun, W.J. Buma, H. Zhang, Chem. Commun. 49 (2013) 3224–3226.
[157] Q. Yuan, Y. Wu, J. Wang, D.Q. Lu, Z.L. Zhao, T. Liu, X.B. Zhang, W.H. Tan, Angew. Chem. Int. Ed. 52 (2013) 13965–13969.
[158] X.J. Zhu, W. Feng, J. Chang, Y.W. Tan, J.C. Li, M. Chen, Y. Sun, F.Y. Li, Nat. Commun. 7 (2016) 10437.
[159] L. Cheng, K. Yang, Y.G. Li, X. Zeng, M.W. Shao, S.T. Lee, Z. Liu, Biomaterials 33 (2012) 2215–2222.
[160] M.E. Davis, Z. Chen, D.M. Shin, Nat. Rev. Drug Discov. 7 (2008) 771–782.
[161] D. Peer, J.M. Karp, S. Hong, O.C. Farokhzad, R. Margalit, R. Langer, Nat. Nanotechnol. 2 (2007) 751–760.
[162] L.B. Peppas, J.O. Blanchette, Adv. Drug Deliv. Rev. 64 (2012) 206–212.
[163] B. Huang, W.Q. Wang, M. Bates, X.W. Zhuang, Science 319 (2008) 810–813.
[164] U.V. Nägerl, K.I. Willig, B. Hein, S.W. Hell, T. Bonhoeffer, Proc. Natl. Acad. Sci. U. S. A. 105 (2008) 18982–18987.
[165] H. Shroff, C.G. Galbraith, J.A. Galbraith, E. Betzig, Nat. Methods 5 (2008) 417–423.
[166] V. Levi, E. Gratton, Cell Biochem. Biophys. 48 (2007) 1–15.
[167] F.Q. Chen, D. Gerion, Nano Lett. 4 (2004) 1827–1832.
[168] L. Liang, J. Li, Q. Li, Q. Huang, J.Y. Shi, H. Yan, C.H. Fan, Angew. Chem. Int. Ed. 53 (2014) 7745–7750.
[169] K. Jaqaman, D. Loerke, M. Mettlen, H. Kuwata, S. Grinstein, S.L. Schmid, G. Danuser, Nat. Methods 5 (2008) 695–702.
[170] G. Ruan, A. Agrawal, A.I. Marcus, S.M. Nie, J. Am. Chem. Soc. 129 (2007) 14759–14766.
[171] M. Howarth, W.H. Liu, S. Puthenveetil, Y. Zheng, L.F. Marshall, M.M. Schmidt, K.D. Wittrup, M.G. Bawendi, A.Y. Ting, Nat. Methods 5 (2008) 397–399.
[172] T. Dertinger, R. Colyer, G. Iyer, S. Weiss, J. Enderlein, Proc. Natl. Acad. Sci. U. S. A. 106 (2009) 22287–22292.
[173] P.A. Frantsuzov, R.A. Marcus,Phys. Rev. B 72 (2005), 155321.
[174] M.X. Yu, F.Y. Li, Z.G. Chen, H. Hu, C. Zhan, H. Yang, C.H. Huang, Anal. Chem. 81 (2009) 930–935.
[175] H.L. Jo, Y.H. Song, J. Park, E.J. Jo, Y.C. Goh, K. Shin, M.G. Kim, K.T. Lee, Nanoscale 7 (2015) 19397–19402.
[176] H. Qian, M.P. Sheetz, E.L. Elson, Biophys. J. 60 (1991) 910–921.
[177] M.J. Saxton, K. Jacobson, Annu. Rev. Biophys. Biomol. Struct. 26 (1997) 373–399.
[178] M.A. Jepson, Adv. Drug Deliv. Rev. 57 (2005) 1–214.
[179] F. Wang, S.H. Wen, H. He, B.M. Wang, Z.G. Zhou, O. Shimoni, D.Y. Jin, Light Sci. Appl. 7 (2018) 18007.
[180] J. Zhou, H.Q. Chu, Y. Zhao, Y. Lu, L.L. Li, J. Am. Chem. Soc. 141 (2019) 7056–7062.
[181] J. Zhao, J.H. Gao, W.T. Xue, Z.H. Di, H. Xing, Y. Lu, L.L. Li, J. Am. Chem. Soc. 140 (2018) 578–581.
[182] Z. Yuan, L. Zhang, S.Z. Li, W.N. Wang, M. Lu, Y. Pan, X.J. Xie, L. Huang, W. Huang, J. Am. Chem. Soc. 140 (2018) 15507–15515.
[183] Y.F. Li, Z.H. Di, J.H. Gao, P. Cheng, C.Z. Di, G. Zhang, B. Liu, X.H. Shi, L.D. Sun, L.L. Li, J. Am. Chem. Soc. 139 (2017) 13804–13810.
[184] K.G. Shah, P. Yager, Anal. Chem. 89 (2017) 12023–12029.
[185] J.M. Lan, Y.X. Liu, F.D. Wen, F. Wu, Z.Z. Han, W.M. Sun, C.Y. Li, J.H. Chen, Sci. Rep. 6 (2016) 24813.
[186] S. Xu, B. Dong, D.L. Zhou, Z. Yin, S.B. Cui, W. Xu, B.J. Chen, H.W. Song, Sci. Rep. 6 (2016) 23406.
[187] Q. Long, Y.Q. Wen, H.T. Li, Y.Y. Zhang, S.Z. Yao, J. Fluoresc. 27 (2017) 205–211.
[188] S.R. Du, J.H. Gil, H. Dong, X.Y. Zheng, G.M. Lyu, M.B. López, J. Gallo, L.D. Sun, C.H. Yan, N.J. Long, Dalton Trans. 46 (2017) 13957–13965.
[189] X. Liu, S.Q. Zhang, X. Wei, T. Yang, M.L. Chen, J.H. Wang, Biosens. Bioelectron. 109 (2018) 150–155.
[190] T. Näreoja, T. Deguchi, S. Christ, R. Peltomaa, N. Prabhakar, E. Fazeli, N. Perälä, J.M. Rosenholm, R. Arppe, T. Soukka, M. Schäferling, Anal. Chem. 89 (2017) 1501–1508.

[191] K.Z. Zheng, Z.Y. Liu, C.J. Lv, W.P. Qin, J. Mater. Chem. C 1 (2013) 5502–5507.
[192] J. Zhang, B.W. Ji, G.B. Chen, Z.H. Hua, Inorg. Chem. 57 (2018) 5038–5047.
[193] L.H. Fischer, G.S. Harms, O.S. Wolfbeis, Angew. Chem. Int. Ed. 50 (2011) 4546–4551.
[194] G.F. Liu, Z. Sun, Z.L. Fu, L. Ma, X.J. Wang, Talanta 169 (2017) 181–188.
[195] A. Sedlmeier, D.E. Achatz, L.H. Fischer, H.H. Gorris, O.S. Wolfbeis, Nanoscale 4 (2012) 7090–7096.
[196] F. Vetrone, R. Naccache, A. Zamarrón, A.J. de La Fuente, F. Sanz-Rodríguez, L.M. Maestro, E.M. Rodriguez, D. Jaque, J.G. Solé, J.A. Capobianco, ACS Nano 4 (2010) 3254–3258.
[197] X.Q. Ge, L.N. Sun, B.B. Ma, D. Ji, L. Dong, L.Y. Shi, N. Li, H.G. Chen, W. Huang, Nanoscale 7 (2015) 13877–13887.
[198] H. Zhu, F. Lu, X.C. Wu, J.J. Zhu, Analyst 140 (2015) 7622–7628.
[199] S. Wu, X.J. Kong, Y. Cen, J. Yuan, R.Q. Yu, X. Chu, Nanoscale 8 (2016) 8939–8946.
[200] K.Y. Zhang, L. Yang, F. Lu, X.C. Wu, J.J. Zhu,Small 14 (2018), 1703858.
[201] S.W. Hell, J. Wichmann, Opt. Lett. 19 (1994) 780–782.
[202] S.W. Hell, T.A. Klar, Opt. Lett. 24 (1999) 954–956.
[203] K.I. Willig, S.O. Rizzoli, V. Westphal, R. Jahn, S.W. Hell, Nature 440 (2006) 935–939.
[204] S.W. Hell, Science 316 (2007) 1153–1158.
[205] U. Resch-Genger, M. Grabolle, S. Cavaliere-Jaricot, R. Nitschke, T. Nann, Nat. Methods 5 (2008) 763–775.
[206] J. Hanne, H.J. Falk, F. Görlitz, P. Hoyer, J. Engelhardt, S.J. Sahl, S.W. Hell, Nat. Commun. 6 (2015) 7127.
[207] B. Buchegger, J. Kreutzer, B. Plochberger, R. Wollhofen, D. Sivun, J. Jacak, G.J. Schütz, U. Schubert, T.A. Klar, ACS Nano 10 (2016) 1954–1959.
[208] R.T. Wu, Q.Q. Zhan, H.C. Liu, X.Y. Wen, B.J. Wang, S.L. He, Opt. Express 23 (2015) 32401–32412.
[209] K. Shin, T. Jung, E. Lee, G. Lee, Y. Goh, J. Heo, M. Jung, E.J. Jo, H. Lee, M.G. Kim, K. Lee, Phys. Chem. Chem. Phys. 19 (2017) 9739–9744.
[210] Y.J. Liu, Y.Q. Lu, X.S. Yang, X.L. Zhang, S.H. Wen, F. Wang, X. Vidal, J.B. Zhao, D.M. Liu, Z.G. Zhou, C.S. Ma, J.J. Zhou, J.A. Piper, P. Xi, D.Y. Jin, Nature 543 (2017) 229–233.
[211] Q.Q. Zhan, H.C. Liu, B.J. Wang, Q.S. Wu, R. Pu, C. Zhou, B.R. Huang, X.Y. Peng, H. Ågren, S.L. He, Nat. Commun. 8 (2017) 1058.
[212] J.A. Delaire, K. Nakatani, Chem. Rev. 100 (2000) 1817–1846.
[213] F.M. Raymo, M. Tomasulo, Chem. Soc. Rev. 34 (2005) 327–336.
[214] D. Dulić, S.J. van der Molen, T. Kudernac, H.T. Jonkman, J.J.D. de Jong, T.N. Bowden, J. van Esch, B.L. Feringa, B.J. van Wees,Phys. Rev. Lett. 91 (2003), 207402.
[215] O. Nevskyi, D. Sysoiev, A. Oppermann, T. Huhn, D. Wöll, Angew. Chem. Int. Ed. 55 (2016) 12698–12702.
[216] M. Irie, T. Fukaminato, T. Sasaki, N. Tamai, T. Kawai, Nature 420 (2002) 759–760.
[217] Z.G. Zhou, H. Hu, H. Yang, T. Yi, K.W. Huang, M.X. Yu, F.Y. Li, C.H. Huang, Chem. Commun. (2008) 4786–4788.
[218] J.N. Liu, W.B. Bu, L.M. Pan, J.L. Shi, Angew. Chem. Int. Ed. 52 (2013) 4315–4379.
[219] L. Zhou, Z.W. Chen, K. Dong, M.L. Yin, J.S. Ren, X.G. Qu, Adv. Mater. 26 (2014) 2424–2430.
[220] B. Yan, J.C. Boyer, D. Habault, N.R. Branda, Y. Zhao, J. Am. Chem. Soc. 134 (2012) 16558–16561.
[221] V. Shanmugam, S. Selvkumar, C.S. Yeh, Chem. Soc. Rev. 43 (2014) 6254–6287.
[222] C.J. Carling, J.C. Boyer, N.R. Branda, J. Am. Chem. Soc. 131 (2009) 10838–10839.
[223] J.C. Boyer, C.J. Carling, B.D. Gates, N.R. Branda, J. Am. Chem. Soc. 132 (2010) 15766–15772.
[224] L. Wang, H. Dong, Y.N. Li, C.M. Xue, L.D. Sun, C.H. Yan, Q. Li, J. Am. Chem. Soc. 136 (2014) 4480–4483.
[225] L. Wang, H. Dong, Y.N. Li, R. Liu, Y.F. Wang, H.K. Bisoyi, L.D. Sun, C.H. Yan, Q. Li, Adv. Mater. 27 (2015) 2065–2069.
[226] J. Lai, Y. Zhang, N. Pasquale, K.B. Lee, Angew. Chem. Int. Ed. 53 (2014) 14419–14423.
[227] K.Z. Zheng, S.Y. Han, X. Zeng, Y.M. Wu, S.Y. Song, H.J. Zhang, X.G. Liu,Adv. Mater. 30 (2018), 1801726.
[228] H. Zhu, X. Chen, L.M. Jin, Q.J. Wang, F. Wang, S.F. Yu, ACS Nano 7 (2013) 11420–11426.
[229] X. Chen, L.M. Jin, W. Kong, T.Y. Sun, W.F. Zhang, X.H. Liu, J. Fan, S.F. Yu, F. Wang, Nat. Commun. 7 (10304) (2016) 1–6.
[230] L.M. Jin, X. Chen, C.K. Siu, F. Wang, S.F. Yu, ACS Nano 11 (2017) 843–849.
[231] T. Wang, H. Yu, C.K. Siu, J.B. Qiu, X.H. Xu, S.F. Yu, ACS Photonics 4 (2017) 1539–1543.
[232] T. Wang, C.K. Siu, H. Yu, Y.F. Wang, S.Q. Li, W. Lu, J.H. Hao, H. Liu, J.H. Teng, D.Y. Lei, X.H. Xu, S.F. Yu, Inorg. Chem. 57 (2018) 8200–8204.
[233] X. Chen, L.M. Jin, T.Y. Sun, W. Kong, S.F. Yu, F. Wang, Small 13 (2017) 1701479.
[234] A. Fernandez-Bravo, K.Y. Yao, E.S. Barnard, N.J. Borys, E.S. Levy, B.N. Tian, C.A. Tajon, L. Moretti, M.V. Altoe, S. Aloni, K. Beketayev, F. Scotognella, B.E. Cohen, E.M. Chan, P.J. Schuck, Nat. Nanotechnol. 13 (2018) 572–577.

Kezhi Zheng earned his B.S. degree in physics from Harbin Normal University in 2005. He received his Ph.D. degree in Physical Electronics from Jilin University in 2011. He then joined the faculty of the Jilin University. He is currently a postdoctoral fellow in the group of Prof. Xiaogang Liu at the National University of Singapore. His current research interests focus on the design and synthesis of lanthanide-doped upconversion materials for emerging applications.

Kang Yong Loh obtained his B.S. degree in Chemistry from the University of Illinois at Urbana-Champaign in 2017 under the supervision of Prof. Yi Lu. He then spent a gap year in the lab of Prof. Xiaogang Liu at the National University of Singapore and the Institute of Materials Research and Engineering (A*STAR). He is currently a Ph.D. graduate student and a Stanford ChEM-H Chemistry/Biology Interface Predoctoral Trainee at Stanford University, Department of Chemistry under the supervision of Prof. Karl Deisseroth. His research interests include developing novel chemical and protein tools to address questions in neuroscience.

Yu Wang earned his BE degree in Jilin University. He completed his master's study in Changchun Institute of Optics, Fine Mechanics and Physics, Chinese Academy of Sciences in 2007 and received his Ph.D. degree from the University of Amsterdam in 2011. After working at the Hong Kong University of Science and Technology as a research fellow, he became a postdoctoral researcher in the group of Prof. Xiaogang Liu at the National University of Singapore in 2013. He joined Shenzhen University In 2016. His research interest focuses on optical spectroscopy and new applications of photon upconversion materials.

Qiushui Chen received his B.Sc. degree in chemistry from Fuzhou University in 2009 and Ph.D. degree in Chemistry from Tsinghua University in 2014. He then joined the group of Prof. Xiaogang Liu as a research fellow in the Department of Chemistry at the National University of Singapore in 2015. His research interests are inorganic luminescence nanocrystals and their use for optical imaging.

Jingyue Fan was born in Sichuan, China. She earned her B.S. degree in 2017 from the National University of Singapore (NUS). She is now pursuing a Ph.D. degree at NUS under the supervision of Professor Xiaogang Liu. Her research interests focus on the synthesis of optical nanomaterials and understanding of energy transport at single-particle levels.

Taeyoung Jung was born in Gumi, Korea, in 1991. He received his B.S. at the Chungnam National University (Daejeon, Korea) in 2014. He is currently a doctorate research student at Gwangju Institute of Science and Technology (GIST) under the supervision of Prof. Kang Taek Lee. During his doctorate research, he worked at the Laboratory for Advanced Molecular Probing (LAMP) in Korea Research Institute of Chemical Technology (KRICT) for two years in 2017–2019 under the supervision of Prof. Dr. Yung Doug Suh. His research mainly focused on lanthanide-doped upconverting nanoparticles and their application in cell biology.

Sang Hwan Nam got his B.S. (2002) in Chemistry from Kyung Hee University, Seoul, Korea and received M.S.(2004) and Ph.D. (2010) in Physical Chemistry from the same university. He joined the Laboratory for Advanced Molecular Probing (LAMP), Korea Research Institute of Chemical Technology (KRICT) as a Researcher in 2009 and worked as a Postdoc Fellow from 2010 to 2013. He was promoted to his current position, a Senior Researcher, at the same lab of KRICT in August 2013. His current research focuses on in vitro and in vivo bioimaging applications of nanomaterials, upconversion nanoparticles (UCNPs), magnetic nanoparticles (MNPs), and Au nanoparticles (AuNPs), as well as the development of high-sensitivity imaging platforms for the disease diagnosis.

Yung Doug Suh studied at Seoul National University for his BS(1991), MS(1993), and PhD(1999) under the guidance of Prof. Seong Keun Kim in Chemistry Department, Prof. Young Kuk in Physics Department, and Dr. Dongho Kim in Korea Research Inst. of Standards and Science (KRISS) researching gas-phase molecular reaction dynamics, surface physics with UHV-STM, and laser spectroscopies, respectively. After finishing his Postdoctoral research in ETH Zurich working with Prof. Renato Zenobi in 1999–2000, where he co-invented TERS(Tip-enhanced Raman Scattering), he worked at the Pacific Northwest Nat'l Laboratory (PNNL), USA, in 2001–2002 doing single-molecule spectroscopy. He accepted a recruited principal research scientist position in 2003, to form his research group, Laboratory for Advanced Molecular Probing (LAMP), at the Korea Research Institute of Chemical Technology (KRICT) in Daejeon, Korea. He is currently a Group Leader at the Research Center for Bio Platform Technology in KRICT, and also serves as a professor at the School of Chemical Engineering in SungKyunKwan Univerisity (SKKU), Korea, since March 2013.

Xiaogang Liu earned his B.E. degree (1996) in Chemical Engineering from Beijing Technology and Business University, P. R. China. He received his M.S. degree (1999) in Chemistry from East Carolina University under the direction of Prof. John Sibert and completed his Ph.D. (2004) at Northwestern University under the supervision of Prof. Chad Mirkin. He then became a postdoctoral fellow in the group of Prof. Francesco Stellacci at MIT. He joined the faculty of the National University of Singapore in 2006. Currently, he sits as an Associate Editor for Nanoscale and serves on the editorial boards of Chemistry—An Asian Journal, Advanced Optical Materials, Journal of Luminescence, and Journal of Physical Chemistry Letters. His research encompasses optical nanomaterials and energy transfer and explores the use of luminescent nanocrystals for photocatalysis, sensing, and biomedical applications.